Geosci. Model Dev. Discuss., 7, 6263–6325, 2014
www.geosci-model-dev-discuss.net/7/6263/2014/
doi:10.5194/gmdd-7-6263-2014

Geoscientific Model Development Discussions
Open Access

Development and basic evaluation of a prognostic aerosol scheme in the CNRM Climate Model

M. Michou, P. Nabat, and D. Saint-Martin

CNRM-GAME, Météo-France, Centre National de Recherches Météorologiques, UMR3589, 42 avenue G. Coriolis, 31057 Toulouse CEDEX 1, France

Received: 12 August 2014 – Accepted: 1 September 2014 – Published: 25 September 2014

Correspondence to: M. Michou (martine.michou@meteo.fr)
and P. Nabat (pierre.nabat@meteo.fr)

Published by Copernicus Publications on behalf of the European Geosciences Union.

Abstract

We have implemented a prognostic aerosol scheme in the CNRM-GAME/CERFACS climate model, based upon the GEMS/MACC aerosol module of the ECMWF operational forecast model. This scheme describes the physical evolution of the five main types of aerosols, namely black carbon, organic matter, sulfate, desert dust and sea-salt. In this work, we describe the specificities of our implementation, for instance, taking into consideration a different dust scheme or boosting biomass burning emissions by a factor of 2, as well as the evaluation performed on simulation outputs. The simulations consist of 2004 conditions and transient runs over the 1993–2012 period, and are either free-running or nudged towards the ERA-Interim Reanalysis. Evaluation data sets include several satellite instrument AOD products (i.e., MODIS Aqua classic and Deep-Blue products, MISR and CALIOP products), as well as ground-based AERONET data and the derived AERONET climatology, MAC-v1. The internal variability of the model has little impact on the seasonal climatology of the AODs of the various aerosols, and the characteristics of a nudged simulation reflect those of a free-running simulation. In contrast, the impact of the new dust scheme is large, with modelled dust AODs from simulations with the new dust scheme close to observations. Overall patterns and seasonal cycles of the total AOD are well depicted with, however, a systematic low bias over oceans. The comparison to the fractional MAC-v1 AOD climatology shows disagreements mostly over continents, while that to AERONET sites outlines the capability of the model to reproduce monthly climatologies under very diverse dominant aerosol types. Here again, underestimation of the total AOD appears in several cases, linked sometimes to insufficient efficiency of the aerosol transport away from the aerosol sources. Analysis of monthly time series at 166 AERONET sites shows, in general, correlation coefficients higher than 0.5 and lower model variance than observed. A large interannual variability can also be seen in the CALIOP vertical profiles over certain regions of the world. Overall, this prognostic aerosol scheme

GMDD
7, 6263–6325, 2014

appears suitable for aerosol-climate studies. There is room, however, for implementing more complex parameterisations in relation to aerosols.

1 Introduction

Tropospheric aerosols strongly influence the climate system (Kaufman et al., 2002), in multiple and complex ways because of interactions with radiation and clouds. They have been known, especially since the 3rd and 4th IPCC reports (Intergovernmental Panel on Climate Change) (IPCC, 2001, 2007), and are still known to contribute largely to the uncertainties in climate system modelling (see the Clouds and Aerosols chapter of the 5th IPCC report, Boucher et al., 2012) for several reasons, as, for instance, the quantification of the aerosol–cloud effects (Lohmann et al., 2005) or the representation of their optical properties (Mallet et al., 2013) continues to be a challenge. A more basic uncertainty can be attributed to the inaccurate representation of aerosol distribution in the atmosphere which is highly variable in space and time because of very diverse aerosol sources, themselves suffering from very different estimations (see e.g., de Leeuw et al., 2011) and of a life time shorter than a few days. This uneven distribution in the atmosphere remains hard to simulate with current climate models (Boucher et al., 2012).

Although a community of global aerosol modellers has been working together for more than 10 years under the AeroCom project (Aerosol Comparisons between Observations and Models), with coordinated simulation exercises analysed in a large number of papers (see Kinne et al., 2006; Textor et al., 2006 as first papers, and http://aerocom.met.no/Welcome.html for a list of publications), aerosol schemes within climate models, such as those used for phase 5 of the Coupled Model Intercomparison Project (CMIP5, Taylor, 2009), are still undergoing development and evaluation (see e.g., Evan et al., 2014). Modelling requires a fundamental understanding of processes and their representation in large-scale models, and a number of climate models

GMDD
7, 6263–6325, 2014

continues to consider prescribed aerosol climatologies. Such climatologies have been continuously upgraded, from Tanré et al. (1984) to Kinne et al. (2013).

More recently, the ACCMIP (Atmospheric Chemistry and Climate Model Intercomparison Project, Lamarque et al., 2013) analysed the aerosol forcing of about 10 free-running global models, in contrast to AeroCom models driven by meteorological analyses, looking at past and future reference periods in coordination with CMIP5 experiments (Lee et al., 2013; Shindell et al., 2013). In general, these ACCMIP models have less sophisticated aerosol physics than the AeroCom models, and the issue of the added value of an explicit aerosol module as part of the climate model is still under debate (Ekman et al., 2014).

We have implemented a prognostic aerosol module within the climate model of Météo-France that takes part in CMIP exercises in order to have the requisite tool to contribute to answering such an issue. This tool will also improve our knowledge about aerosol-climate interactions. In this paper, we provide a description and an evaluation of this aerosol module. We describe the underlying General Circulation Model (GCM) and the aerosol scheme in Sect. 2, the simulation performed together with the evaluation data used in Sect. 3, and the results from our evaluation, with firstly intrinsic specificities of our simulations, and then confrontation between simulation outputs and observed data sets in Sect. 4.

2 Description of the aerosol scheme

2.1 The underlaying GCM

The aerosol scheme has been included as one of the physical packages of the ARPEGE-Climat GCM. ARPEGE-Climat is the atmospheric component of the CNRM-GAME (Centre National de Recherches Météorologiques – Groupe d'études de l'Atmosphère Météorologique) and CERFACS (Centre Européen de Recherche et de

GMDD
7, 6263–6325, 2014

Formation Avancée) coupled Atmosphere-Ocean General Circulation Model (AOGCM) CNRM-CM, whose development started in the 1990s.

We present in this work an evaluation of the aerosol scheme driven by version 6.1 (v6.1) of ARPEGE-Climat that is an evolution of v5.2, fully described in Voldoire et al. (2012), and used to contribute to CMIP5. ARPEGE-Climat v6.1 is based on the dynamical core cycle 37 of the ARPEGE-Integrated Forecast System (IFS) Météo-France/European Centre for Medium-Range Weather Forecasts (ECMWF) operational numerical weather forecast models. The major differences between v5.2 and v6.1 consist of differences in their respective physics: that of v5.2 is described in Voldoire et al. (2012), while the specificities of v6.1 are in summary as follows: the vertical diffusion scheme is a prognostic turbulent kinetic energy scheme (Cuxart et al., 2000), where the microphysics is the detailed prognostic scheme of Lopez (2002), used both for the large-scale and convective precipitation. The shallow and deep convection are those of the Prognostic Condensates Microphysic Transport (PCMT) scheme described in Piriou et al. (2007); Guérémy (2011). Further details on ARPEGE-Climat, valid for both versions 6.1 and 5.2, which concern for instance the radiation scheme, appear in Voldoire et al. (2012). The surface parameters of ARPEGE-Climat have been computed with the external surface scheme, SURFEX (v7.3), already in place for CMIP5 simulations. SURFEX can consider a diversity of surface formulations for the evolution of four types of surface: nature, town, inland water and ocean. A description of SURFEX is available in the overview paper of Masson et al. (2013), from the simple to the quite complex parameterisations available. We considered for this paper a configuration of SURFEX very close to the one presented in Voldoire et al. (2012), except for the air–sea turbulent fluxes that are those of the COARE 3.0 iterative algorithm (Fairall et al., 2003; Masson et al., 2013).

The interactive aerosol scheme presented below is aimed at replacing the description of the tropospheric aerosols currently in place in ARPEGE-Climat, which was used for the CMIP5 simulations and consists of 2-D monthly climatologies of the AOD (Aerosol Optical Depth) of five types of aerosols, namely sea salt (SS), desert dust

GMDD
7, 6263–6325, 2014

(DD), black carbon (BC), organic matter (OM) and sulfate (SO_4) aerosols, with a vertical profile depending on the aerosol type (see Voldoire et al., 2012).

The ARPEGE-Climat configuration used here is the one that CNRM and CERFACS scientists have agreed to probably serve as the basic configuration for future CMIP6 simulations: the ARPEGE-Climat spectral model is operated in a T127 triangular truncation, with the physics calculated onto a reduced Gaussian grid equivalent to a spatial resolution of about 1.4° in both longitude and latitude. The vertical description consists of 91 hybrid sigma pressure levels defined by the ECMWF, as already adopted in a number of studies with ARPEGE-Climat (e.g., Guérémy, 2011), which include 9 layers below 500 m and 52 layers below 100 hPa, ensuring a correct description of the vertical distribution of the tropospheric aerosols, from the surface with the aerosols emissions up to the middle troposphere where the concentration of most aerosols reaches very low values. A time step of 15 min is used for the model integration.

2.2 The original GEMS/MACC aerosol scheme

The prognostic aerosol scheme of ARPEGE-Climat is based upon the GEMS/MACC aerosol description included in the ARPEGE/IFS ECMWF operational forecast model starting in 2005 as part as the European projects Global and regional Earth system Monitoring using Satellite and in situ data (GEMS, 2005–2009, Hollingsworth et al., 2008) and its follow-up projects Monitoring Atmospheric Composition and Climat (MACC, MACC-II, 2009-, http://www.gmes-atmosphere.eu/), which provide a pre-operational atmospheric environmental service to complement the weather analysis and forecasting services of European and national organisations by addressing the composition of the atmosphere.

The GEMS/MACC aerosol scheme describes the physical evolution of the five main types of tropospheric aerosols mentioned previously (Morcrette et al., 2009), in which various "bins" are considered: sea-salt discriminates 3 size-bins particles (radius boundaries of 0.03–0.5, 0.5–5, 5–20 µm); desert dust also has 3 size-bins (0.03–0.5, 0.5–0.9, 0.9–20 µm); the boundaries given are for dry particles, however, the ambient

GMDD
7, 6263–6325, 2014

humidity is taken into account in the computation of the aerosol optical properties; organic matter and black carbon separate a hydrophilic and a hydrophobic component; and for the representation of sulfate both a sulfate precursor, named SO_2, and a sulfate aerosol, named SO_4, cohabit in the scheme. Hence the aerosol scheme adds up 12 prognostic variables to the original prognostic meteorological variables.

The scheme allows a number of physical evolutions of the aerosols, including dry deposition at the surface, assuming constant dry deposition velocities as a function of the aerosol and of the surface type (land, ocean, ice); sedimentation with a settling velocity depending on the aerosol "bin"; hygroscopic growth of BC and OM, assuming that OM is distributed between 50 % hydrophilic and 50 % hydrophobic when emitted, whereas BC is distributed between 80 % hydrophilic and 20 % hydrophobic when emitted; wet deposition in and below clouds, from large-scale and convective precipitation, with release of aerosols when precipitation re-evaporates in the atmosphere; and conversion from SO_4 precursors into SO_4 that does not consider any chemical species, but is done along with an exponential function, with a time constant depending on the latitude. Sources of SS and DD are calculated at each model integration using model meteorological fields. For SS, an emission flux is considered only over full ocean grids, and for their open ocean fraction only excluding a possible sea ice fraction, as a function of the wind speed at the model lowest level. The SS mass flux is tabulated depending on the wind speed class, based on work from Guelle et al. (2001) (see other references in Morcrette et al., 2009). For DD, the parameterisation is derived from that of Ginoux et al. (2001). DD is produced over selected model grids cells, i.e., snow free, fractions of bare soil/high and low vegetation above/below given thresholds respectively, and depends on the soil upper layer wetness, the albedo, the model's lowest level wind speed and the particle radius. For the other aerosols, OM, BC and the SO_4 precursors, external monthly inventories are read in. The aerosol scheme separates between the biomass burning source, in order to allow for real-time updates of that source in the IFS model (see for instance Kaiser et al., 2012), and all the other sources (e.g., fossil fuel, natural sources). The inventories used for our simulations and for the MACC

GMDD
7, 6263–6325, 2014

Reanalysis performed with the IFS system are presented respectively in Sects. 2.3.3 and 3.2.1.

Finally concerning their physical evolution, large-scale and parameterized transports of the prognostic aerosols, e.g. convective and diffusive transports, are done by the ARPEGE-Climat code in the same way as for any meteorological prognostic field (see Sect. 2.1).

A detailed description of the original GEMS/MACC aerosol scheme appears in Morcrette et al. (2009), and the list of parameters of the scheme, together with the values used for the MACC Reanalysis (see Sect. 3.2.1), is given in Table 4. These parameters are fully detailed in Morcrette et al. (2009), and for the sake of clarity parameter names in Table 4 correspond to the ones in Morcrette et al. (2009). Other papers related to this GEMS/MACC scheme address improvements of the scheme (Morcrette et al., 2008), the aerosol assimilation system fully integrated into the ECMWF assimilation apparatus (Benedetti et al., 2009), the Global Fire Assimilation System that calculates in real-time aerosol biomass burning emissions by assimilating observations from the MODIS instruments (Kaiser et al., 2012), evaluation of all or individual aerosol distributions (Morcrette et al., 2009, 2011a, b; Huneeus et al., 2011; Mangold et al., 2011), and finally estimations of the GEMS/MACC aerosol radiative forcing (Bellouin et al., 2012).

2.3 Implementation of the aerosol scheme in ARPEGE-Climat

2.3.1 Adaptation of the scheme

Preliminary simulations with the original configuration of the aerosol scheme, with the same static emissions for BC, OM and SO_4 precursors as those for IFS runs, lead to aerosol concentrations much lower than the ones issued from IFS runs (not shown). As the literature presents a range of values for the various coefficients listed in Table 4, we adopted the values that would maximise the concentrations in ARPEGE-Climat runs. These new values are shown in red in Table 4. The efficiency of scavenging rates corresponds to the lowest values of Textor et al. (2006), whereas we got the deposition

GMDD
7, 6263–6325, 2014

velocities from Huneeus et al. (2007) and Reddy et al. (2005) and the settling sedimentation velocities from Huneeus et al. (2007). One has to note that in this newer version of the aerosol scheme, the sedimentation process is applied only to the coarser bins of SS and DD, SSbin03 and DDbin03 in Table 4, as suggested in Huneeus et al. (2009). Additional information for sulfate and its precursors comes from Boucher et al. (2002). Lastly, the hydrophilic/hydrophopic fraction of BC has been corrected from an incorrect value, we now have a fraction of 0.8/0.2 in place of the original fraction of 0.2/0.8, and the radii of the three dust bins have been modified (P. Nabat, personal communication, 2013), with 0.32–0.75–9.0 µm and 0.2–1.67–11.6 µm mean bin radii respectively in the GEMS/MACC and our versions.

In addition to the adaptations presented above, developments have been made in the vertical diffusion and mass-flux convection schemes of ARPEGE-Climat (see Sect. 2.1) to account explicitly for the sub-grid transport of tracers.

2.3.2 Inclusion of an additional dust scheme

Based on preliminary results using the original GEMS/MACC dust scheme, and as a more complex scheme could be put into place in view of the detailed parameters on the soil characteristics available in ARPEGE-Climat from the ECOCLIMAP database (Masson et al., 2003), an additional dust emission parameterisation has been included in the aerosol scheme, allowing for comparisons between the two schemes. This dust emission parameterisation comes from Marticorena and Bergametti (1995), which is very common in aerosol global models and takes into account soil information such as the erodible fraction and the fractions of sand and clay. The horizontal saltation flux is calculated as a function of the soil moisture, the surface roughness length and the wind velocity at the model's lowest level. The vertical flux is then inferred from this saltation flux, and the emitted dust size distribution is based on the work of Kok (2011). More details about this dust emission parameterisation can be found in Nabat et al. (2012, 2014c). Note that the normalized constant c_α listed in Nabat et al. (2012) had to be adjusted to the horizontal resolution of our simulations to a value of $c_\alpha = 5 \times 10^{-7}$.

GMDD
7, 6263–6325, 2014

2.3.3 Specificities of our "static" emissions

The basis for our "static" emissions is the ACCMIP/AEROCOM emission inventory obtained from ftp://ftp-ipcc.fz-juelich.de/pub/accmip/gridded_netcdf/accmip_interpolated, fully presented and referred as the A2-ACCMIP data set in Diehl et al. (2012), and used in other publications (e.g., Chin et al., 2014; Pan et al., 2014).

The A2-ACCMIP emissions are derived, for BC, primary organic carbon (OC), and SO_2, the major sulfate precursor, from the Lamarque et al. (2010) inventory developed for the Intergovernmental Panel on Climate Change Fifth Assessment Report. The original Lamarque et al. (2010) 1850–2000 inventory, from land-based anthropogenic sources and ocean-going vessels, in decadal increments, has been interpolated for A2-ACCMIP into yearly increments and extended beyond 2000 with the RCP8.5 (Representative Concentration Pathways) future emission scenario (Riahi et al., 2011).

The A2-ACCMIP biomass burning emissions of BC, OM and SO_2 are those of the ACCMIP/MACCity biomass burning data set, which contains monthly mean emissions with explicit interannual variability and which is the original data set used to construct the decadal mean ACCMIP biomass burning emissions (Granier et al., 2011). ACCMIP/AEROCOM emissions are originally at a $0.5^\circ \times 0.5^\circ$ resolution.

Apart from these anthropogenic sources, natural emissions of aerosols include sulfur contributions from volcanoes and oceans (Boucher et al., 2002; Huneeus et al., 2007), and Secondary Organic Aerosols (SOA) formed from natural Volatile Organic Compound (VOC) emissions. We considered the SO_2 from volcanoes described in Andres and Kasgnoc (1998), which is a yearly climatology of both continuous degassing and explosive volcanoes (1° horizontal resolution). The Kettle et al. (1999) dimethylsulfide (DMS) climatology, emitted from the oceans, has the same temporal and spatial characteristics as the Andres and Kasgnoc (1998) volcano data set, and is therefore independent from the surface meteorological conditions in our simulations. A review of DMS inventories, available from http://www.geiacenter.org/access/geia-originals, indicates that the Kettle et al. (1999) data set served as the basis for other DMS inventories,

GMDD
7, 6263–6325, 2014

and is still a valid data set to use. And finally, as our emissions scheme does not describe the SOA formation, we prescribed the SOA inventory of Dentener et al. (2006), representative of the year 2000. Therefore, all three data sets, SO_2 from volcanoes, DMS and SOA, do not have any interannual variability.

As in Boucher et al. (2002); Huneeus et al. (2007), we added an H_2S source as an additional sulfate precursor, which we scaled to the SO_2 source (5 %), and we considered a direct emission of sulfate (5 % of the emitted SO_2, Benkovitz et al., 1996).

As preliminary simulations of BC and OM revealed that our modeled related AODs were biased low, and keeping in mind a possible overestimation of our aerosol sinks noting that the option was rejected by Kaiser et al. (2012) who also worked with the Morcrette et al. (2009) model, we chose to augment our emissions by applying scaling factors to them. This appears to be quite a common practice in the aerosol modelling community, e.g. for BC and OM see Kaiser et al. (2012); Tosca et al. (2013), and for SOA see Tsigaridis et al. (2014). Noting that a factor of 1.5 exists between OC emissions, as provided in the Juelich data set, and OM emissions (see Kaiser et al. (2012) or Chin et al. (2014) and references therein), we present results in this paper having applied a factor of 2 to the original Juelich BC and OM biomass burning emissions, and to the Dentener et al. (2006) SOA inventory. We computed this scaling factor from MISR and MODIS observations over the two major biomass burning regions of South America and Southern Africa to bring our 2004 AODs into reasonable agreement with the satellite data. Note that, unlike in Tosca et al. (2013), we did not apply factors depending on the region. Finally we also rescaled the sulfate precursor emissions, excepted from the biomass burning source, with a factor of 0.7.

The emissions are injected into the surface layer of ARPEGE-Climat, which is about 20 m thick in our 91 level configuration, and quickly distributed throughout the boundary layer by model processes such as convection and vertical diffusion. We limited the OM surface emissions to $5 \times 10^{-9}\,kg\,m^{-2}\,s^{-1}$, and the BC and SO_2 emissions to $5 \times 10^{-10}\,kg\,m^{-2}\,s^{-1}$, as higher values, reached during very intensive biomass burning

GMDD
7, 6263–6325, 2014

events or volcanic eruptions, generated unrealistic high AOD (higher than 10) in the model. This limitation has a small impact on the monthly or yearly total emissions.

The resulting yearly totals emitted appear in Table 2, distinguishing the biomass burning, the natural and the other sources. Total emissions are higher in our simulations than in the MACC Reanalysis (see further details on the MACC Reanalysis emissions in Sect. 3.2.1) for all aerosols, but all our totals are in within the ranges provided by the literature (see also Table 2). Both the intra and inter-annual variabilities come from the biomass burning emissions (not shown), with the biomass burning sources representing 49 %, 54 %, and 3 % of the total sources for BC, OM and sulfate precursor emissions respectively in 2004, which is the reference year chosen for four of our simulations (see Sect. 3.1).

3 Simulations performed and evaluation data used

3.1 Simulations

The simulations performed (see Table 1 for a summary) include firstly an ARPEGE-Climat simulation with 2004 conditions for all forcing, namely SST, GHG gases and climatologies of aerosols. This climatology of aerosols is the one that interacts with the radiation scheme of ARPEGE-Climat, as in the CMIP5 simulations (see Voldoire et al., 2012; Szopa et al., 2012), and such a configuration allows an evaluation of the prognostic aerosol distribution independently from their possible impact on the meteorology. This simulation, referred as the FreSim simulation, has been repeated over 10 years to account for the internal variability of the climate model. A second simulation consists in a nudged ARPEGE-Climat simulation, with a spectral nudging (see Douville, 2009) of wind, temperature, humidity and surface pressure applied every 6 h towards the year 2004 of the ERA-Interim Reanalysis (Dee et al., 2011). The motivation for this nudged simulation is twofold: first, as classically in nudged simulations (Zhang et al., 2011), the nudging towards a meteorological reanalysis ensures that the simulated large-scale

GMDD
7, 6263–6325, 2014

circulation is close to the observations and thus the comparison of modelled aerosols is the most realistic one. Second, comparing our free-running and nudged simulations will allow to estimate some possible weaknesses of the free-running simulations. In this simulation, which is called NudSim, nudging is applied to the entire atmosphere and all model levels, with a transition zone from the surface over the last five model levels, the nudging strength being fixed at a 6 h e-folding time. Nudging, or not, the humidity, led to quite different aerosol distributions, and we present here results where nudging of the humidity is applied. Two other simulations, i.e., FreSimd2 and NudSimd2 are identical to FreSim and NudSim except for the dust scheme, which is the one described in Sect. 2.3.2. Lastly, two transient simulations, with corresponding transient forcings, FreSimd2_Trans and NudSimd2_Trans, have been performed with the dust scheme of Sect. 2.3.2 over 1993–2012. This period covers the years of the MACC Reanalysis as well as the satellite and AERONET data that are our evaluation sets (see Sect. 3.2). NudSimd2_Trans has been nudged towards the ERA-Interim Reanalysis of 1993–2012 as with NudSim.

Another difference between the free-running and the nudged ARPEGE-Climat simulations, apart from their specific meteorology, is that release of aerosols in the course of stratiform precipitation re-evaporation is not applied to the free-running simulations. Such a release led to a limited number of abnormally high AODs, which was sufficient to perturb local AODs during a couple of weeks. This issue is not caused by the wet deposition formulation itself, but appears to be linked to the characteristics of specific meteorological conditions along the vertical axis, which we do not encounter in the nudged simulations.

3.2 Evaluation data

3.2.1 The MACC Reanalysis data

The MACC Reanalysis, as part as the MACC FP-7 project is a 10 year long reanalysis of chemically reactive gases and aerosols using a global model and a data assimilation

GMDD
7, 6263–6325, 2014

system based on the ECMWF IFS (see Inness et al., 2013). Its aerosol scheme is that described in Morcrette et al. (2009), so it is similar to the scheme evaluated here, and its aerosol assimilation system uses MODIS AOD (Benedetti et al., 2009). Anthropogenic aerosol emissions are described in Granier et al. (2011), while the biomass burning emissions take advantage of the Global Fire Assimilation System (GFAS) of MACC that rests upon daily fire radiative power information from the MODIS instruments (Kaiser et al., 2012; Inness et al., 2013). The Reanalysis used, as we did, the SOA climatology of Dentener et al. (2006), but did not consider any sulfur emissions from volcanos or oceans, and no specific direct H_2S or sulfate emissions.

The MACC Reanalysis was performed onto 60 vertical hybrid sigma-pressure levels, with a model top at 0.1 hPa, and a T255 spectral truncation corresponding to a reduced Gaussian grid with a horizontal resolution of approximately 80 km. Analyses of the characteristics of the simulated aerosols during this 10 year Reanalysis appear in various papers including those of Bellouin et al. (2012); Melas et al. (2013); Nabat et al. (2013); Cesnulyte et al. (2014).

3.2.2 Satellite and ground-based data

We used several observation data sets that complement each other. The satellite data were obtained from the NASA Langley Research Center Atmospheric Science Data Center, and consist firstly of the MODerate resolution Imaging Spectroradiometer (MODIS), on board the Aqua satellite that is largely used in the modelling aerosol community. We used the level-3 collection 5.1 total AOD at 550 nm monthly product over the 10 year period 2003–2012 (see Tanré et al., 1997; Levy et al., 2007) at 1° resolution, and the similar product derived from the "Deep-Blue" algorithm developed to get aerosol optical thickness over bright land areas (Hsu et al., 2004). In addition, as there exist a variety of satellite aerosol products that may disagree, as analysed for instance in Bréon et al. (2011); Nabat et al. (2013), we included in our analysis AOD data from the Multiangle Imaging SpectroRadiometer (MISR) (Kan et al., 2005, 2010) on board

GMDD
7, 6263–6325, 2014

the Terra satellite. The MISR monthly product has the same horizontal resolution as MODIS and covers the period 2001–2012.

The Cloud-Aerosol Lidar with Orthogonal Polarization (CALIOP), on board the Aerosol Lidar and Infrared Pathfinder Satellite Observations (CALIPSO) satellite, is one of the very few satellite instruments providing vertical information on the aerosol distribution. We used a level-3 global monthly gridded (1°) 3-D CALIOP product that covers the years 2006–2011, courtesy of B. Koffi, already introduced at the end of the Koffi et al. (2012) paper, and under final evaluation (see Koffi, 2014 and references therein). Extinction coefficients are provided at various wavelengths, under clear sky and all sky conditions, on a 1° resolution grid, every 100 m from the surface up to 10 km, for all aerosols and also distinguishing the dust component. We made analysis with the 532 nm products, in all sky conditions as Koffi et al. (2012) indicates that "the climatology of the mean aerosol vertical extinction distribution is not significantly affected by the presence of clouds."

The AErosol RObotic NETwork (AERONET) is a ground-based globally distributed network of automatic sun photometer measurements of aerosol optical properties every 15 min, that is a reference for AOD measurements (see Holben et al., 1998). For the present work, we used AOD monthly average quality-assured data (Level 2.0, see Holben et al., 2006) downloaded from the AERONET website (http://aeronet.gsfc.nasa.gov). Multiannual monthly averages are available from 1993, and we retained in our analysis stations that included five years, or more, of total AOD at various spectral bands, from which we recomputed the total AOD at 550 nm when missing in the original data set, using theÅngström coefficient. AERONET AOD data have a high accuracy of < 0.01 for wavelengths longer than 440 nm and < 0.02 for shorter wavelengths (Holben et al., 1998). We derived monthly time series and a representative station climatology from 166 AERONET stations over the world that represent areas under the influence of various dominant aerosols.

The Max-Planck-Institute Aerosol Climatology (MAC-v1) AEROCOM/AERONET climatology of aerosol optical properties takes advantage of developments in aerosol

GMDD
7, 6263–6325, 2014

modeling and in aerosol observational capabilities. It relies on information provided by the global network of ground based sun-photometers, mostly from the AERONET network (see above), together with an ensemble of model outputs of the AEROCOM experiments. The climatology includes estimates from pre-industrial (1860) to 2100 conditions, and distinguishes between fine and coarse mode aerosols, the former with a radius from 0.05 to 0.5 microns that mostly include particles issued from gas to particle conversion, while the latter, with a radius of up to 15 microns, include essentially sea salt and lifted soil-dust aerosols. It includes monthly timescale data with global coverage at a spatial resolution of 1°. Temporal evolution distinguishes between anthropogenic aerosols that include interannual changes while natural aerosols consider only seasonal variations. For further details see Kinne et al. (2013).

4 Results

4.1 Some characteristics of the ARPEGE-Climat simulations

4.1.1 Internal variability

As a preliminary compulsory step before any further analysis of the simulations, we looked at the stability over time of the aerosol scheme. Figure 1 shows time series of mean global monthly concentrations, in the 1000–500 hPa layer, of the 12 prognostic aerosol "bins" over a period common to the MACC Reanalysis and our transient simulations (2003–2012). Aside from these multi-year simulations, the diagrams include pseudo time-series of the FreSim simulation that repeated 10 times the 2004 conditions.

Overall, all simulations, both nudged or free-running, show no drift over time of the aerosol concentrations. Starting with an initial state with no prognostic aerosols, equilibrium of aerosol concentrations is reached in ARPEGE-Climat simulations within the period of a month (not shown).

GMDD
7, 6263–6325, 2014

Figure 2 displays the interannual standard deviation (STD) of the AOD (total and five main aerosols) for JJA and the FreSimd2 simulation. This STD is a representation of ARPEGE-Climat internal variability, and we present this simulation and this season as the STD for the FreSim simulation has similar characteristics to those of the FreSImd2 simulation, and as the response of the model for the DJF season is lower for all aerosols than that for the JJA season.

STD > 0.01 are always under 20 to 30 % of the corresponding mean value, for all aerosols (not shown). Standard deviation of the total AOD is rarely higher than 0.05, with the highest values in the biomass burning regions of Central South America (SAM) and Africa (SAF), and over west of India (IND), which corresponds with larger STDs for OM and DD (see Fig. 2). Further insight on the internal variability of ARPEGE-Climat total AOD is provided with figures of vertical profiles of extinction coefficients for total aerosols (see Figs. 15 and 16) and for dust aerosols (see Fig. 17). A description and analysis of these figures appear in Sect. 4.2.3, but for the matter of interest in this paragraph we can say that larger STD in the SAF and SAM regions, related to the diverse spread of biomass burning aerosols (i.e., OM and BC), and in the Indian region (IND) in conjunction with variability in wet scavenging, appear to be consigned to altitudes below 3–4 km. In contrast, STD of extinction coefficients of the central Atlantic (CAT) region, fully explained by the values and spread in dust extinction coefficients (see Fig. 17) is quite large, up to 5 kms. Overall, the interannual STD of the FreSimd2 simulation is lower, for all sub-regions of the globe and for both seasons than that of the CALIOP extinction profile product.

Overall, we can conclude from this short analysis that the internal variability of ARPEGE-Climat has little impact on the seasonal climatology of the AODs, both considering all or individual aerosols.

4.1.2 The nudged vs. free-running simulations

As relative differences in AOD between nudged and free-running simulations appear independent of the dust scheme (not shown), we will discuss results for the simulations

GMDD
7, 6263–6325, 2014

with the new scheme only. Figure 1 is a first illustration of the relative behaviour of the nudged (blue lines) vs. free-running (green lines) simulations. Global monthly means of aerosol concentrations from these two types of simulations appear as distinct curves except for 3 "bins", namely the hydrophobic OM and BC, and the sulfate precursor. In the FreSimd2_Trans and NudSimd2_Trans simulations, these 3 "bins" share several common characteristics of their physical evolution, including no wet scavenging, no sedimentation, a dry deposition independent from the meteorology, and the same static emissions. The specific meteorologies of these two simulations, that govern sub-grid scale and large-scale transport, appear then to have little impact on the global mean monthly concentrations of these 3 "bins". For the other "bins", values are in general higher for the nudged simulation, in agreement with lower wet scavenging due to lower precipitation (not shown), and to the release of aerosols in the case of re-evaporation of precipitation, release suppressed for the free-running simulation (see Sect. 3.1). However, the case of sea-salt, with global means lower for the NudSimd2_Trans simulation, illustrates the relative importance of the various sources and sinks: with both lower dynamical emissions for DD and SS in the nudged simulation (by about 15 %, see Table 3), DD concentrations are higher in the nudged simulation while SS concentrations are lower. An explanation for that is the smaller importance of wet scavenging on total losses for SS than for DD, with efficiencies for scavenging of respectively 0.2 and 0.5 (see Table 4).

Figure 3 displays differences in AOD between the NudSimd2 and the FreSimd2 simulations, for DJF and JJA of 2004. Over most of the globe, absolute differences in total AOD (first row of the figure) are lower than 0.05. However, differences are higher than 0.2 in DJF over central Africa, and in JJA over eastern Africa, the Indian Ocean and small spots in biomass burning regions such as Indonesia. For the former these absolute differences come from differences in the OM AOD (see second row) in relation to differences in precipitation patterns (not shown) that impact the wet scavenging in this region and season of large biomass burning, while for the latter differences in total AOD mimic those in DD AOD (see third row), with higher dust emissions in conjunction

GMDD
7, 6263–6325, 2014

with higher winds (not shown). In the end, differences in AODs between a free-running and a nudged ARPEGE-Climat simulation appear relatively small.

4.1.3 Impact of the dust scheme

Table 3 presents the mean annual dust emissions in various regions of the globe, from our four simulations of the year 2004 (see Table 1), the MACC Reanalysis, and the 15 AEROCOM global models analysed in Huneeus et al. (2011). The regions are also those of Huneeus et al. (2011). The AEROCOM range for the globe (min and max) is wide (e.g., 487–3943 $\mathrm{Tg\,yr^{-1}}$), but the NudSimd2 simulation is the only one that falls within that range, the FreSimd2 simulations modelling higher emissions, and the other three simulations modelling lower emissions. Totals in the regions may not been consistently high (respectively low) within the same model, and our NudSimd2 simulation shows totals for the Middle East and Australia outside of the AEROCOM ranges, with particularly large emissions in Australia. This suggests that further adjustments of the scheme should be studied, and a simple adjustment could concern, for instance, the threshold of proportion of bare soil within a grid cell required to trigger DD emissions. Such adjustments would depend on the underlying meteorology; the impact of the lowest level and surface meteorology is clearly seen with global emissions of the NudSimd2 simulation being only about 85 % of the corresponding simulation with ARPEGE-Climat meteorology (i.e., FreSimd2 simulation).

Total DD emissions are multiplied by a factor of 14 by this change of emission scheme (NudSim vs. NudSimd2 simulation), knowing that factors are of 2.8, 2.9 and 20.9 for the DDbin01, DDbin02 and DDbin03 respectively. The corresponding changes in AOD, for the three dust bins and the total dust aerosol are shown in Fig. 4. In the end, the mean global total DD AOD is enhanced by 4.7.

GMDD
7, 6263–6325, 2014

4.1.4 ARPEGE-Climat simulations vs. the MACC Reanalysis

Evaluations of climate models against reanalysis outputs are very common practice. The MACC Reanalysis is all the more interesting to us as we make use of a twin brother aerosol scheme, and as we can access in the ECMWF MARS archive diagnoses that are less common than the AODs, such as 3-D individual "bin" concentrations. Evaluation results about the MACC Reanalysis indicate that the MACC system generally provides a good representation of the AOD on a monthly basis (Cesnulyte et al., 2014). However, a few deficiencies have been underlined such as dust being associated to too small particles, and thus being overly transported to regions very remote from the sources. Another deficiency is that sea salt seems to be overestimated and contributes to a high AOD bias in southern oceanic regions (Melas et al., 2013).

The results of the comparison between our model outputs and the MACC Reanalysis are the following, noting that for BC comparisons between the MACC Reanalysis and our simulations cannot be made fairly as a wrong $\frac{\text{hydrophilic}}{\text{hydrophobic}}$ fraction is present in the MACC Reanalysis (see Table 4).

Global means of tropospheric "bin" concentrations are shown in Fig. 1 for the MACC Reanalysis (red lines) and the NudSimd2_Trans simulation (blue lines). Concentrations of the various bins from our simulations are biased low compared to the MACC Reanalysis, except for the hydrophobic bins, this being possibly linked to the suppression of wet scavenging in our scheme (see Table 4), and, linked to our new dust scheme, for the three dust bins. Modifications of the constants of the aerosol scheme to trigger higher concentrations (see Sect. 2.3.1), in parallel with enhancement of static emissions (see emission totals in Table 2), resulted in these very different global monthly means. Differences in sea-salt concentrations are particularly striking.

Analysis of lat-lon plots of AODs (see Fig. 5) reveals that transport away from the sources is more efficient with the MACC Reanalysis meteorology than with the meteorological conditions of our nudged simulation. In the end, lower global mean values of the NudSimd2_Trans simulation in Fig. 1 are caused by lower concentrations away

GMDD
7, 6263–6325, 2014

from the source regions. This is the case for all smaller aerosols with no or little sedimentation, and is clearly visible for instance for BC, OM and sulfate. In the case of SS, in addition to long-range transport within continents characteristic of the MACC Reanalysis, concentrations or AODs are larger in the MACC Reanalysis even at the source regions with higher emissions (64.2 vs. 51.6 Pg year^{-1}). However, as SS of the MACC Reanalysis seems to be overestimated (see above), we chose to go along in this paper with our modeled SS distributions.

Finally, these results can also be explained by the role of the aerosol assimilation present in the MACC Reanalysis that significantly modifies aerosol concentrations and improves agreement with observations as compared to control runs without aerosol assimilation (Kaiser et al., 2012; Melas et al., 2013).

In summary to conclude this Sect. 4.1, as we demonstrated that (1) in a climatological perspective ARPEGE-Climat free-running and nudged simulations show little differences, and (2) the new dust scheme performs much better than the original one, we will then go along in the remainder of this paper with analysis of the NudSimd2_Trans simulation only against observations.

4.2 ARPEGE-Climat simulations vs. satellite and ground-based data

4.2.1 Total AOD

Figures of total AOD (Figs. 6 and following) show DJF and JJA means over 2003–2012 of the three satellite data sets, i.e., MODIS Aqua standard and Deep-Blue products and MISR, of our NudSimd2_Trans simulation, and of the Kinne et al. (2013) climatology representative of the year 2000. The main spatial patterns as well as the local seasonal cycles of the total AOD in various regions of the globe, in conjunction for instance with JJA dust emissions in Northern Africa or the Middle East, or biomass burning in Central Africa, or sea salt production in the southern oceans, are clearly depicted by the model. However, overall model outputs underestimate satellite observations, noting that the three satellite data sets may greatly disagree over large areas. This

GMDD
7, 6263–6325, 2014

model underestimation is lower in JJA than in DJF, with a relative mean bias between MISR and the simulation of 47 and 56 %, respectively (see Figs. 8 and 9). This low bias is mainly driven by the oceanic values. In contrast, the model overestimates the observations in DJF in areas such as Central Africa, parts of Saudi Arabia and Northern Africa. Areas of model overestimation seem to follow the trace of biomass burning in tropical regions. Over continents in JJA, at mid to northern latitudes, the bias appears quite patchy, with both positive and negative values.

Relative biases between model outputs and the other two satellite data sets, i.e. the MODIS Aqua and the Deep Blue products, yielded different results. MISR and MODIS differ by more than than 20 % over large parts of the oceans, and they contrast even more over continents. The same comment applies to MODIS Deep Blue over continents, and is even more true for the Kinne et al. (2013) climatology. Over mid to high latitude oceans, the bias between Kinne et al. (2013) and our simulation is lower (around 10 to 50 %, not shown) than the bias between MISR and our simulation (around 30 to 70 %).

4.2.2 Fractional AOD

Figure 10 shows several fractions of the annual mean total AOD, for the Kinne et al. (2013) climatology, representative of the year 2000, and the NudSimd2 simulation. Fractions are those available in Kinne et al. (2013), and we grouped our aerosol scheme "bins" to comply to the extent possible to these fractions. Total AOD has been separated in AOD from the coarse mode (the two largest of the three bins of SS and DD in our simulations), the fine mode, that complements the coarse mode, the anthropogenic sulfate aerosols (in our case sulfate from all sources, including natural sources such as oceans or volcanoes), and the natural aerosols (in our case DD and SS aerosols).

Higher coarse-mode AODs are associated with dust (e.g. Northern Africa) and sea salt (e.g., Southern oceans), whereas higher fine-mode AOD contributions are registered over regions of urban pollution and regions affected by biomass burning. As these

GMDD
7, 6263–6325, 2014

two modes complement each other, a model underestimation of the former goes with a model overestimation of the latter, and vice-versa. In general, the model underestimates the coarse mode fraction over continents (by 40 % or more), except for the very northern part of Africa, the Mongolian desert region, and the tropical Pacific ocean.

The sulfate fractions of the total AODs of Kinne et al. (2013) and the NudSimd2 simulation show similarities in their hemispheric repartition, with fractions lower than 0.3 in most of the Southern Hemisphere. Over Europe and the United States, however, our fractions appear too high (by more than two times). This is also the case over regions in pristine air affected only by volcanoes, such as the Hawaiian Islands or the Antarctic continent (Mount Erebus volcano), which is coherent with the Kinne et al. (2013) sulfate fraction consisting of anthropogenic sulfate only.

Finally, the fraction of natural aerosols is correctly simulated over the oceans and dust-producing regions. Over the rest of the continents, we underestimate this fraction as we could not include in this fraction the contribution from second organic aerosols, which are not a simulation output.

To go further in the evaluation of the various fractions of the total AOD, Fig. 12 presents, for the selection of twelve AERONET stations as in Cesnulyte et al. (2014), the monthly climatological AOD at 550 nm, computed over all years of data available at each given AERONET station. The NudSimd2_Trans aerosol "bin" AODs, at the locations of the AERONET sites, appear in the same figure grouped into SS, DD, OM, BC and SO_4 AODs, in addition to the AERONET total AOD, and allow then for an evaluation of the various fractions of the total AOD. These AERONET sites cover various parts of the globe (see Fig. 11 for their locations), and are categorized in three groups depending on the typically dominating aerosol type: urban/anthropogenic for the Ispra, Kanpur, La Jolla, Thessaloniki and XiangHe sites; biomass burning for the Alta Floresta and Mongu sites; and dust for the Capo Verde, El Arenosillo, Ilorin, La Parguera and Solar Village sites.

The annual cycle of the total AOD is generally well represented by the model, with either a unique narrow peak during the year, such as at the biomass burning site of

GMDD
7, 6263–6325, 2014

Alta Floresta in South America, or a peak over several months such as at the dust site of Solar Village in Saudi Arabia, or two peaks as in Kanpur North India, which coincide with the pre and post-monsoon seasons. The model is also able to capture the range of AODs covered by this selection of areas, going from total AODs lower than 0.2 all year round at La Jolla or El Arenosillo, to medium AODs (around 0.5 in Capo Verde), and to large AODs of 1 (Alta Floresta). Another characteristic of the model outputs is that, in almost all cases, the model shows a nul to low bias compared to the observations.

The low bias is particularly important for the Ispra site (mean yearly bias-MB of 0.13), with sulfate as the dominant aerosol all year round in observations (Cesnulyte et al., 2014), as it is also the case in the model outputs. However, underestimation of model sulfate here is in disagreement with the overestimation of the sulfate fraction in comparison to the Kinne et al. (2013) climatology described earlier in this section. This underestimation could be questioned as the data quality score of Kinne et al. (2013) is moderate only for this ISPRA site, the remaining of the Cesnulyte et al. (2014) sites having an excellent quality score. Furthermore, the two nearby sites at the regional scale, Thessaloniki and El Arenosillo, show much better agreement between the model and the observed climatologies, even though the dust and sulfate contributions differ for all three sites, as for instance El Arenosillo can be affected by dust storms from Northern Africa.

The two Asian sites of Kanpur and XiangHe are also affected by high pollution, and large observed AODs (larger than 0.4) prevailing all year round are underestimated in our simulation by a factor of ~ 2. Underestimation is even larger at Ilorin (MB = 0.4), located in sub-Saharan Africa, particularly in the dry season months from November to April. This site is obviously under dust storms, but Cesnulyte et al. (2014) indicate that fine aerosol from biomass burning make a significant contribution during this dry season, which is a contribution that we seem to be underestimating.

At the two shore/ocean sites of La Jolla (Pacific shore) and of La Parguera (Caribbean Islands), with relatively clean air all year round (total AOD lower than 0.25), the model underestimation appears related to an underestimation of the dust AOD, with

GMDD
7, 6263–6325, 2014

dust transported from the nearby Mojave or further away Saharan deserts, respectively (Cesnulyte et al., 2014).

Nevertheless, agreement between model and observations is particularly good at the two biomass sites of Alta Floresta in South America and of Mongu in South Africa, which is more of a savannah region. This is also the case at the two dust sites of Solar Village, in the heart of the Arabian Peninsula, with a small negative MB of −0.05, and of Capo Verde located ∼ 730 km of the Senegal coast. The dust transport seems well represented here, although slightly underestimated (MB = 0.11).

As an overall performance of the NudSimd2_Trans simulation, we present in Fig. 13 a Taylor diagram (Taylor, 2001) computed from the time series of the 166 AERONET stations we retained in our analysis (see Sect. 3.2.2) and of the corresponding simulation outputs at the station location. These time series could in principle cover the 1993–2013 period, but the time period covered is shorter in most cases. Stations have been qualified according to the dominant aerosol type (ocean, mountain, polar, biomass, coastal, dust, polluted, and land, see Kinne et al., 2013). The most common locations are land (46 stations), coastal (26), and polluted (25). For graphical purposes, negative correlation coefficients have been set to zero, and normalized standard deviations higher than 1.75 have been set to 1.75. Overall, the model performs rather satisfactorily with regards to the time correlation between observed and modelled values: the majority of series have correlation coefficients higher than 0.5 (118 stations). With regards to the variability of the series, the diagram reports on the ratio between model and observed standard deviations, and indicates that this ratio is below 0.5 for a significant number of stations (47). However, this ratio is higher than 1 for the same number of stations.

To further illustrate the behaviour of the model at the monthly time scale, Fig. 14 shows monthly times series, with the same representation of the AOD as in Fig. 12, over all years of data available at a given AERONET site. Included is a selection of six stations performing particularly “badly” according to the Taylor diagram of Fig. 13, followed by a selection of stations performing “well” ($CC > 0.5$ and $0.5 < rVAR < 1.5$).

GMDD
7, 6263–6325, 2014

According to Kinne et al. (2013), all of these stations have a quality score of 3 (excellent), and a representativeness score varying between 900 km to 100 km. This selection addresses several dominant aerosol types and locations in the world (see Fig. 11).

Out the 166 total AERONET sites none of the 5 sites qualified as ocean sites perform "well". The Bermuda thumbnail illustrates that here again: as in the La Parguera case (see above in the same section), the model misses higher levels of AOD. The Dhadnah and Grande SONDA cases (qualified as performing "well") confirm the good climatologies seen for the relatively "near-by" stations of Solar Village and Alta Floresta of Cesnulyte et al. (2014). In these regions the model appears to perform correctly over large areas. The same comment can apply to the Taihu station in China, and the correspondent station of Xianghe in Cesnulyte et al. (2014), changing performing "well" to "badly".

In contrast, while the three stations of IMS-METU-ERDEMLI, OHP_OBSERVATOIRE, and Bersk perform badly, either because of a poor CC, or a poor rVar, the Moldova station located in the same region of the world performs well. This underlines the challenge of modelling aerosols in that Euro-Mediterranean region (Nabat et al., 2013, 2014a, b, c). The case of Arica, with a MB of 0.22 and an rVar of 0.08 requires further investigation (specificities/representativity/quality of the site) that goes beyond the scope of this paper. And to finish on this comparison, particularly difficult for a climate model, the two cases of Halifax and Lake Argyle, with very different repartitions of the total AOD, but with similarly good results, are encouraging.

4.2.3 Vertical evaluation

Figures 15 and 16 display mean vertical profiles of total extinction coefficients (km^{-1}) for DJF and JJA, respectively, averaged for individual years. These years cover the 2006–2011 period for the CALIOP instrument, and are representative of the 2004 year for the FreSimd2 simulation (previously mentioned in Sect. 4.1.1) and the NudSimd2 simulation. We output vertical information to compare with the CALIOP data from these two simulations only. Profiles are presented for the 12 regions displayed in Koffi et al.

GMDD
7, 6263–6325, 2014

(2012), representative of regions with a dominance of marine aerosols (NAT, CAT and NWP regions), of industrial aerosols (EUS, WEU, IND and ECN regions), of dust aerosols (NAF and WCN regions), and of biomass burning aerosols (SAM, CAF, and SAF regions). In addition to these figures, Fig. 17 shows vertical profiles of dust extinction coefficients (km^{-1}), for the same simulations/observations as Figs. 15 and 16, for DJF and JJA, and for the six Koffi et al. (2012) regions with a significant contribution of dust aerosols to total aerosols.

In general, model outputs are biased low compared to the CALIOP data, except for the North Africa region (NAF), which presents a quasi-nul bias in DJF and a positive bias between 0.03 and 0.09 km^{-1} depending on the altitude. The seasonality in the vertical profiles of NAF and CAT appears clearly in the model and in the observations, with dust at higher levels due to transport from easterly winds reaching up to 6 km, and advection of the Saharan dust to the Atlantic between 2 and 5 km (see Fig. 16).

The model's low bias is particularly marked for the CAT, WCN, SAF and IND regions. For CAT, the marine boundary layer aerosol load is clearly underestimated in both seasons. This is also the case for the marine NWP region in JJA, but this marine aerosol load is correctly simulated in the North Atlantic (NAT) region. For the dust area of Mongolia (WCN), Koffi et al. (2012) indicate that significant CALIOP vs. MODIS AOD discrepancies are obtained e.g., for the WCN West China dust region DJF bias = +128 % and SON bias = +74 %. Particularly high inter-annual variability observed for this WCN region could be due both to its reduced size and to the high variability of the processes responsible for the uplift of the dust particles. Koffi et al. (2012) report a particularly large inter-model (12 model analysed) range for this region of WCN in DJF, probably linked to unresolved processes such as wind gusts, which are not taken into account in our dust emission schemes. The Southern Hemisphere biomass burning South Africa (SAF) low extinction profiles result probably in JJA from an underestimation of the fires, although vertical transport of the fire aerosols appears clearly in the characteristic seasonal shape of the profiles. Koffi et al. (2012) indicate that a potential factor contributing to aerosol at high altitudes is the formation of secondary aerosols from the biomass

GMDD
7, 6263–6325, 2014

burning gaseous products during plume aging. This process is not represented in our aerosol scheme.

The convex character of the mean JJA profiles in SAF for example (see Fig. 16) is, however, rather well depicted by the model. Finally, for the Indian industrial region (IND), the NudSimd2 simulation generates an S curve shape in JJA that appears quite unique and could be related to an overly large wet deposition sink.

Figure 17, which depicts dust only extinction profiles, provides further insight into the model behaviour: the North Africa (NAF) profiles in Fig. 17, when compared to the profiles of Figs. 15 and 16 confirm that dust is the predominant aerosol in that entire region. This also appears to be the case, although to a lesser extent, in the boundary layer for the Western China (WCN) region in DJF, but is not at all the case for the other regions and/or seasons. Agreement between model and observations is correct for WEU, with very low extinction coefficients, for CAF in DJF and finally for CAT in the 2–4 km layer in JJA.

5 Conclusions

We have introduced a prognostic aerosol scheme within the atmospheric component ARPEGE-Climat of the climate model of CNRM/GAME – CERFACS climate model (Voldoire et al., 2012). Until now, aerosol AODs were prescribed to the model as monthly AODs.

This scheme is based on the GEMS/MACC aerosol module included in the ARPEGE/IFS ECMWF operational forecast model from 2005 (Morcrette et al., 2009), which describes the physical evolution of the five main types of aerosols, BC, OM, DD, SS and sulfate. A total of 12 bins are distinguished in the parameterisations of the physical evolution of the aerosols, which include dry and wet deposition, sedimentation, hygroscopic growth, conversion for sulfate precursors into sulfate, and dynamical emissions of dust and sea salt. Large and sub-grid scale (i.e., diffusion and convection)

GMDD
7, 6263–6325, 2014

transports of these additional prognostic fields of the atmospheric model are also considered.

We implemented a number of changes in the original scheme, such as modifications of the constants involved in the various parameterisations and addition of a new dust emission scheme based on Marticorena and Bergametti (1995); Kok (2011). Furthermore, biomass burning emissions of OM and BC and emissions of SOA have been rescaled (Kaiser et al., 2012; Tsigaridis et al., 2014), as a common practice in aerosol modelling, by a factor of 2. These changes were aimed at enhancing preliminary low concentrations from our simulations.

We performed a number of simulations to evaluate different aspects of our modelling of aerosols such as the internal variability of the climate model, the behaviour of free-running simulations vs. nudged simulations, and the sensitivity to the dust emission scheme. Then, transient (1993–2012) simulations were aimed at validating the model, in a climatological way, from the seasonal to the monthly time scale, against satellite observations, available over the entire or part of the 2003–2012 period, against in-situ AERONET measurements, available, depending on the site as from 1993, and against the Kinne et al. (2013) global climatology that relies on information from the AERONET stations.

The internal variability of the model has little impact on the seasonal climatology of the AODs of the various aerosols. Differences in AODs between a free-running and a nudged simulations appear lower than 0.05 over most of the globe. Higher differences (> 0.2) exist in conjunction with large AODs of biomass burning emitted OM in DJF or of dust in JJA. In the end, the performance of a nudged simulation is comparable to that of a free-running simulation.

Analysis of simulations differing by the dust emission scheme alone revealed large differences in both emission fluxes and dust AODs. For the former, global dust emissions are multiplied by 14, realising that this factor is dependant on the region. This factor varies also according to the dust bin size, and to this end global mean dust AOD is enhanced by a factor of 4.7.

GMDD
7, 6263–6325, 2014

Spatial distribution of aerosol concentrations and resulting AODs of, on the one hand, the MACC Reanalysis of reactive gases and aerosols and, on the other hand, our simulations are quite dissimilar, even though the two underlying GCMs share very close aerosol modules. Higher emissions, both dynamic and "static", and parameters of the aerosol scheme tuned to reduce aerosol sinks resulted in much lower aerosol concentrations (AODs) away from the source regions in our simulations.

Overall patterns and seasonal cycles of the total AOD are well depicted by our nudged transient simulation when compared to the satellite AOD. Over oceans, however, the simulation has a systematic low bias, of varying importance depending on the observational data set. Over continents, differences are more diverse with patches of low and high biases.

We compared portions of the total simulated AOD with the fractions described in the Kinne et al. (2013) climatology. In general, the model underestimates both coarse and the natural fractions over continents, except over dust-emitting areas. For the natural fraction, this could reflect different aerosols types being considered within the category. On parallel, it appears to overestimate the sulfate fraction over industrialised countries of the Northern Hemisphere.

Evaluation of the various aerosol types has also been performed against AERONET observations of total AOD at 550 nm. Monthly climatologies computed over all years of data available at a given site have been examined at the 12 sites of Cesnulyte et al. (2014). The very diverse annual cycles of the total AOD, with varying dominant aerosol types, are well represented by the model. However, the model shows systematically a low to null bias compared to AERONET observations. Underestimation seems to be linked to missing local sources such as biomass burning, or missing more distant sources such as dust transported over the entire Atlantic ocean. Biases are close to 0 at true biomass burning or dust sites.

To go further in qualifying/quantifying the aerosol prognostic scheme, monthly time series of the 166 AERONET sites that add up to 5 years or more of measurements have been compared to model outputs at the corresponding grid cells. The majority

GMDD
7, 6263–6325, 2014

of series have correlation coefficients higher than 0.5, but generally lower variance for the model. Selected time series confirm the difficulty in modelling aerosol at the local scale, but outline also the good performance of the model in certain cases.

Finally, an evaluation of the vertical profile has been performed comparing seasonal, total and dust, extinction coefficients from the CALIOP instrument (2006–2011) and from the model, over the regions analysed in Koffi et al. (2012). The model generally has a low bias, except for the North Africa region where the bias is high. The distinct shape and seasonality of the profiles are rather well represented by the model. A couple of regions appear really hard to simulate (e.g., the Western China WCN region), but there the CALIOP interannual variability is very large.

The evaluation described here indicates that this prognostic aerosol scheme is suitable for aerosol-climate studies. We suggest that remaining issues could be addressed by improving aerosol distributions over oceans. This could result from a different sea-salt emission scheme, or by considering a parameterisation of DMS emissions. Over continents, apart that there is room for improvement in the modelling of SOA, the inclusion of a simple sulfur cycle, considering prescribed monthly distributions of chemical constituents (e.g., OH, or O_3), could yield to better concentrations of sulfate, which is of primary interest to climate.

Acknowledgements. This work was supported by Météo-France, CNRS and CERFACS. We particularly acknowledge the support of the team in charge of the CNRM-GAME/CERFACS climate model. We are also grateful to J.-J. Morcrette for many very helpful discussions and advice over several years. Supercomputing time was provided by Météo-France/DSI supercomputing center. MODIS used in this paper were retrieved from the Giovanni online data system, developed and maintained by the NASA GES DISC. MISR data were obtained from the NASA Langley Research Center Atmospheric Science Data Center, and AERONET data from the http://aeronet.gsfc.nasa.gov web site. We would like to thank B. Koffi, J. Griesfeller and M. Schulz for providing access to CALIOP data from the AeroCom server. We also thank S. Kinne and A. Heil for advice on the Kinne et al. (2013) climatology and on the A2-ACCMIP emissions inventory respectively. GEMS was funded by the European Commission between 2004 and 2009 as part of the 6th Framework Programme under contract number

GMDD
7, 6263–6325, 2014

SIP4-CT-2004–516099, MACC was funded between 2009 and 2011 as part of the 7th Framework Programme, pilot core GMES Atmospheric Service under contract number 218793, and MACC-II since 2011 as part of the 7th Framework Programm under grant agreement n.283576. ECMWF ERA-Interim data and MACC Reanalysis data used in this study have been provided by ECMWF. We thank E. Paul for his help on the emission and AERONET data processing, and on the displaying of results. Figures have been done using the NCL graphic packages, and some of them with the CCMVal Diagnostic Tool. Finally, we are grateful to L. Watson for her kind advice on the nuances of the English language.

References

Andres, R. J. and Kasgnoc, A. D.: A time-averaged inventory of subaerial volcanic sulfur emissions, J. Geophys. Res., 103, 25251–25261, doi:10.1029/98JD02091, 1998. 6272

Bellouin, N., Quaas, J., Morcrette, J.-J., and Boucher, O.: Estimates of aerosol radiative forcing from the MACC re-analysis, Atmos. Chem. Phys., 13, 2045–2062, doi:10.5194/acp-13-2045-2013, 2013. 6270, 6276

Benedetti, A., Morcrette, J.-J., Boucher, O., Dethof, A., Engelen, R. J., Fisher, M., Flentje, H., Huneeus, N., Jones, L., Kaiser, J. W., Kinne, S., Mangold, A., Razinger, M., Simmons, A. J., and Suttie, M.: Aerosol analysis and forecast in the European Centre for Medium-Range Weather Forecasts Integrated Forecast System: 2. Data assimilation, J. Geophys. Res., 114, D13205, doi:10.1029/2008JD011115, 2009. 6270, 6276

Benkovitz, C. M., Scholz, M. T., Pacyna, J., Tarrason, L., Dignon, J., Voldner, E. C., Spiro, P. A., Logan, J. A., and Graedel, T. E.: Global gridded inventories of anthropogenic emissions of sulfur and nitrogen, J. Geophys. Res., 101, 29239–29253, 1996. 6273

Boucher, O., Pham, M., and Venkataraman, C.: Simulation of the atmospheric sulfur cycle in the LMD GCM: model description, model evaluation, and global and European budgets, Note 23, 26 pp., Inst. Pierre-Simon Laplace, Paris, France, available at: http://icmc.ipsl.fr/index.php/scientific-notes, 2002. 6271, 6272, 6273

Boucher, O., Randall, D., Artaxo, P., Bretherton, C., Feingold, G., Forster, P., Kerminen, V.-M., Kondo, Y., Liao, H., Lohmann, U., Rasch, P., Satheesh, S. K., Sherwood, S., Stevens, B., and Zhang, X. Y.: Clouds and aerosols, in: Climate Change 2013: The Physical Science Basis. Contribution of Working Group I to the Fifth Assessment Report of the Intergovern-

GMDD
7, 6263–6325, 2014

mental Panel on Climate Change, edited by: Stocker, T. F., Qin, D., Plattner, G.-K., Tignor, M., Allen, S. K., Boschung, J., Nauels, A., Xia, Y., Bex, V., and Midgley, P. M., Cambridge University Press, Cambridge, UK and New York, NY, USA, 2013. 6265

Bréon, F.-M., Vermeulen, A., and Descloitres, J.: An evaluation of satellite aerosol products against sunphotometers measurements, Remote Sens. Environ., 115, 3102–3111, doi:10.1016/j.rse.2011.06.017, 2011. 6276

Cesnulyte, V., Lindfors, A. V., Pitkänen, M. R. A., Lehtinen, K. E. J., Morcrette, J.-J., and Arola, A.: Comparing ECMWF AOD with AERONET observations at visible and UV wavelengths, Atmos. Chem. Phys., 14, 593–608, doi:10.5194/acp-14-593-2014, 2014. 6276, 6282, 6285, 6286, 6287, 6288, 6292, 6320

Chin, M., Diehl, T., Tan, Q., Prospero, J. M., Kahn, R. A., Remer, L. A., Yu, H., Sayer, A. M., Bian, H., Geogdzhayev, I. V., Holben, B. N., Howell, S. G., Huebert, B. J., Hsu, N. C., Kim, D., Kucsera, T. L., Levy, R. C., Mishchenko, M. I., Pan, X., Quinn, P. K., Schuster, G. L., Streets, D. G., Strode, S. A., Torres, O., and Zhao, X.-P.: Multi-decadal aerosol variations from 1980 to 2009: a perspective from observations and a global model, Atmos. Chem. Phys., 14, 3657–3690, doi:10.5194/acp-14-3657-2014, 2014. 6272, 6273

Cuxart, J., Bougeault, P., and Redelsperger, J.-L.: A turbulence scheme allowing for mesoscale and large eddy simulations, Q. J. Roy. Meteor. Soc., 126, 1–30, doi:10.1002/qj.49712656202, 2000. 6267

Dee, D. P., Uppala, S. M., Simmons, A. J., et al.: The ERA-Interim reanalysis: configuration and performance of the data assimilation system, Q. J. Roy. Meteor. Soc., 137, 553–597, doi:10.1002/qj.828, 2011. 6274

de Leeuw G., Andreas, E. L., Anguelova, M. D., Fairall, C. W., Lewis, E. R., O'Dowd, C., Schulz, M., and Schwartz, S. E.: Production flux of sea spray aerosol, Rev. Geophys., 49, RG2001, doi:10.1029/2010RG000349, 2011. 6265

Dentener, F., Kinne, S., Bond, T., Boucher, O., Cofala, J., Generoso, S., Ginoux, P., Gong, S., Hoelzemann, J. J., Ito, A., Marelli, L., Penner, J. E., Putaud, J.-P., Textor, C., Schulz, M., van der Werf, G. R., and Wilson, J.: Emissions of primary aerosol and precursor gases in the years 2000 and 1750 prescribed data-sets for AeroCom, Atmos. Chem. Phys., 6, 4321–4344, doi:10.5194/acp-6-4321-2006, 2006. 6273, 6276

Diehl, T., Heil, A., Chin, M., Pan, X., Streets, D., Schultz, M., and Kinne, S.: Anthropogenic, biomass burning, and volcanic emissions of black carbon, organic carbon, and SO_2 from

GMDD
7, 6263–6325, 2014

1980 to 2010 for hindcast model experiments, Atmos. Chem. Phys. Discuss., 12, 24895–24954, doi:10.5194/acpd-12-24895-2012, 2012. 6272

Douville, H.: Stratospheric polar vortex influence on Northern Hemisphere winter climate variability, Geophys. Res. Lett., 36, L18703, doi:10.1029/2009GL039334, 2009. 6274

Ekman, A. M. L.: Do sophisticated parameterizations of aerosol–cloud interactions in CMIP5 models improve the representation of recent observed temperature trends?, J. Geophys. Res.-Atmos., 119, 817–832, doi:10.1002/2013JD020511, 2014. 6266

Evan, A. T., Flamant, C., Fiedler, S., and Doherty, O., An analysis of aeolian dust in climate models, Geophys. Res. Lett., 41, doi:10.1002/2014GL060545, online first, 2014. 6265

Fairall, C. W., Bradley, E. F., Hare, J. E., Grachev, A. A., and Edson, J. B.: Bulk parameterization of air–sea fluxes: updates and verification for the COARE algorithm, J. Climate, 16, 571–591, 2003. 6267

Ginoux, P., Chin, M., Tegen, I., Prospero, J., Holben, B. N., Dubovik, O., and Lin, S.-J.: Sources and distributions of dust aerosols simulated with the GOCART model, J. Geophys. Res., 106, 20255–20274, 2001. 6269, 6305

Guérémy, J. F.: A continuous buoyancy based convection scheme: one- and three-dimensional validation, Tellus A, 63, 687–706, doi:10.1111/j.1600-0870.2011.00521.x, 2011. 6267, 6268

Granier, C., Bessagnet, B., Bond, T., D'Angiola, A., Denier Van Der Gon, H., Frost, G. J., Heil, A., Kaiser, J. W., Kinne, S., Klimont, Z. S. Kloster, Lamarque, J.-F., Liousse, C., Masui, T., Meleux, F., Mieville, A., Ohara, T., Raut, J.-C., Riahi, K., Schultz, M. G., Smith, S. J., Thompson, A., van Aardenne, J., van der Werf, G. R., and van Vuuren, D. P.: Evolution of anthropogenic and biomass burning emissions of air pollutants at global and regional scales during the 1980–2010 period, Climatic Change, 109, 163–190, 2011. 6272, 6276

Grythe, H., Ström, J., Krejci, R., Quinn, P., and Stohl, A.: A review of sea-spray aerosol source functions using a large global set of sea salt aerosol concentration measurements, Atmos. Chem. Phys., 14, 1277–1297, doi:10.5194/acp-14-1277-2014, 2014. 6307

Guelle, W., Schulz, M., Balkanski, Y., and Dentener, F.: Influence of the source formulation on modeling the atmospheric global distribution of the sea salt aerosol, J. Geophys. Res., 106, 27509–27524, 2001. 6269

Holben, B. N., Eck, T. F., Slutsker, I., Tanré, D., Buis, J. P., Setzer, A., Vermote, E., Reagan, J. A., Kaufman, Y., Nakajima, T., Lavenu, F., Jankowiak, I., and Smirnov, A.: AERONET-A Federated Instrument Network and Data Archive for Aerosol Char1205 acterization, Remote Sens. Environ., 66, 1–16, doi:10.1016/S0034-4257(98)00031-5, 1998. 6277

GMDD
7, 6263–6325, 2014

Holben, B. N., Eck, T. F., Slutsker, I., Smirnov, A., Sinyuk, A., Schafer, J., Giles, D., and Dubovik, O.: AERONET's version 2.0 quality assurance criteria, in: Remote Sensing of the Atmosphere and Clouds, Proc. SPIE, 6408, 64080Q, doi:10.1117/12.706524, 2006. 6277

Hollingsworth, A., Engelen, R. J., Benedetti, A., Dethof, A., Flemming, J., Kaiser, J. W., Morcrette, J.-J., Simmons, A. J., Textor, C., Boucher, O., Chevallier, F., Rayner, P., Elbern, H., Eskes, H., Granier, C., Peuch, Rouil, L., and Schultz, M. G.: The Global Earth-system Monitoring using Satellite and in-situ data (GEMS) project: Towards a monitoring and forecasting system for atmospheric composition, B. Am. Meteorol. Soc., 89, 1147–1164, doi:10.1175/2008BAMS2355.1, 2008. 6268

Houghton, J. T., Ding, Y., Griggs, D. J., Noguer, M., van der Linden, P. J., and Xiaosu, D.: Climate Change: The Scientific Basis, contribution of Working Group I to the Third Assessment Report of the Intergovernmental Panel on Climate Change (IPCC), Cambridge University Press, UK, 2001. 6265

Huneeus, N.: Assimilation variationnelle d'observations satellitaires dans un modèle atmosphérique d'aérosols, thèse Université Lille 1 – Sciences et technologies, 2007. 6271, 6272, 6273

Huneeus, N., Boucher, O., and Chevallier, F.: Simplified aerosol modeling for variational data assimilation, Geosci. Model Dev., 2, 213–229, doi:10.5194/gmd-2-213-2009, 2009. 6271

Huneeus, N., Schulz, M., Balkanski, Y., Griesfeller, J., Prospero, J., Kinne, S., Bauer, S., Boucher, O., Chin, M., Dentener, F., Diehl, T., Easter, R., Fillmore, D., Ghan, S., Ginoux, P., Grini, A., Horowitz, L., Koch, D., Krol, M. C., Landing, W., Liu, X., Mahowald, N., Miller, R., Morcrette, J.-J., Myhre, G., Penner, J., Perlwitz, J., Stier, P., Takemura, T., and Zender, C. S.: Global dust model intercomparison in AeroCom phase I, Atmos. Chem. Phys., 11, 7781–7816, doi:10.5194/acp-11-7781-2011, 2011. 6270, 6281, 6307

Huneeus, N., Chevallier, F., and Boucher, O.: Estimating aerosol emissions by assimilating observed aerosol optical depth in a global aerosol model, Atmos. Chem. Phys., 12, 4585–4606, doi:10.5194/acp-12-4585-2012, 2012. 6306

Hsu, N. C., Tsay, S.-C., King, M., and Herman, J. R.: Aerosol properties over bright-reflecting source regions, IEEE T. Geosci. Remote, 42, 557–569, doi:10.1109/TGRS.2004.824067, 2004. 6276

Inness, A., Baier, F., Benedetti, A., Bouarar, I., Chabrillat, S., Clark, H., Clerbaux, C., Coheur, P., Engelen, R. J., Errera, Q., Flemming, J., George, M., Granier, C., Hadji-Lazaro, J., Huijnen, V., Hurtmans, D., Jones, L., Kaiser, J. W., Kapsomenakis, J., Lefever, K., Leitão, J.,

GMDD
7, 6263–6325, 2014

Razinger, M., Richter, A., Schultz, M. G., Simmons, A. J., Suttie, M., Stein, O., Thépaut, J.-N., Thouret, V., Vrekoussis, M., Zerefos, C., and the MACC team: The MACC reanalysis: an 8 yr data set of atmospheric composition, Atmos. Chem. Phys., 13, 4073–4109, doi:10.5194/acp-13-4073-2013, 2013. 6276

IPCC: Climate Change 2007: Synthesis Report. Contribution of Working Groups I, II and III to the Fourth Assessment Report of the Intergovernmental Panel on Climate Change, core writing team, edited by: Pachauri, R. K. and Reisinger, A., IPCC, Geneva, Switzerland, 2007. 6265

Kaiser, J. W., Heil, A., Andreae, M. O., Benedetti, A., Chubarova, N., Jones, L., Morcrette, J.-J., Razinger, M., Schultz, M. G., Suttie, M., and van der Werf, G. R.: Biomass burning emissions estimated with a global fire assimilation system based on observed fire radiative power, Biogeosciences, 9, 527–554, doi:10.5194/bg-9-527-2012, 2012. 6269, 6270, 6273, 6276, 6283, 6291

Kahn, R. A., Gaitley, B. J., Martonchik, J. V., Diner, D. J., Crean, K. A., and Holben, B.: Multiangle imaging spectroradiometer (misr) global aerosol optical depth validation based on 2 years of coincident aerosol robotic network (aeronet) observations, J. Geophys. Res., 110, D10S04, doi:10.1029/2004JD004706, 2005. 6276

Kahn, R. A., Gaitley, B. J., Garay, M. J., Diner, D. J., Eck, T. F., Smirnov, A., and Holben, B. N.: Multiangle Imaging SpectroRadiometer global aerosol product assessment by comparison with the Aerosol Robotic Network, J. Geophys. Res., 115, D23209, doi:10.1029/2010JD014601, 2010. 6276

Kaufman, Y. J., Tanré D., and Boucher, O.: A satellite view of aerosols in the climate system, Nature, 419, 215–223, 2002. 6265

Kettle, A. J., Andreae, M. O., Amouroux, D., Andreae, T. W., Bates, T. S., Berresheim, H., Bingemer, H., Boniforti, R., Curran, M. A. J., DiTullio, G. R., Helas, G., Jones, G. B., Keller, M. D.: A global database of sea surface dimethylsulfide (DMS) measurements and a simple model to predict sea surface DMS as a function of latitude, longitude and month, Global Biogeochem. Cy., 13, 399–444, 1999. 6272

Kinne, S., Schulz, M., Textor, C., Guibert, S., Balkanski, Y., Bauer, S. E., Berntsen, T., Berglen, T. F., Boucher, O., Chin, M., Collins, W., Dentener, F., Diehl, T., Easter, R., Feichter, J., Fillmore, D., Ghan, S., Ginoux, P., Gong, S., Grini, A., Hendricks, J., Herzog, M., Horowitz, L., Isaksen, I., Iversen, T., Kirkevåg, A., Kloster, S., Koch, D., Kristjansson, J. E., Krol, M., Lauer, A., Lamarque, J. F., Lesins, G., Liu, X., Lohmann, U., Montanaro, V.,

GMDD
7, 6263–6325, 2014

Myhre, G., Penner, J., Pitari, G., Reddy, S., Seland, O., Stier, P., Takemura, T., and Tie, X.: An AeroCom initial assessment – optical properties in aerosol component modules of global models, Atmos. Chem. Phys., 6, 1815–1834, doi:10.5194/acp-6-1815-2006, 2006. 6265

Kinne, S., O'Donnel, D., Stier, P., Kloster, S., Zhang, K., Schmidt, H., Rast, S., Giorgetta, M., Eck, T. F., and Stevens, B.: MAC-v1: a new global aerosol climatology for climate studies, J. Adv. Model. Earth Syst., 5, 704–740, doi:10.1002/jame.20035, 2013. 6266, 6278, 6283, 6284, 6285, 6286, 6287, 6288, 6291, 6292, 6293, 6314, 6316, 6318, 6321

Koffi, B., Schulz, M., Bréon, F.-M., Griesfeller, J., Winker, D., Balkanski, Y., Bauer, S., Berntsen, T., Chin, M., Collins, W. D., Dentener, F., Diehl, T., Easter, R., Ghan, S., Ginoux, P., Gong, S., Horowitz, L. W., Iversen, T., Kirkevåg, A., Koch, D., Krol, M., Myhre, G., Stier, P., and Takemura, T.: Application of the CALIOP layer product to evaluate the vertical distribution of aerosols estimated by global models: AeroCom phase I results, J. Geophys. Res., 117, D10201, doi:10.1029/2011JD016858, 2012. 6277, 6288, 6289, 6293, 6323, 6325

Kok, J. F.: A scaling theory for the size distribution of emitted dust aerosols suggests climate models underestimate the size of the global dust cycle, Proc. Natl. Acad. Sci. USA, 108, 1016–1021, 2011. 6271, 6291, 6305

Lamarque, J.-F., Bond, T. C., Eyring, V., Granier, C., Heil, A., Klimont, Z., Lee, D., Liousse, C., Mieville, A., Owen, B., Schultz, M. G., Shindell, D., Smith, S. J., Stehfest, E., Van Aardenne, J., Cooper, O. R., Kainuma, M., Mahowald, N., McConnell, J. R., Naik, V., Riahi, K., and van Vuuren, D. P.: Historical (1850–2000) gridded anthropogenic and biomass burning emissions of reactive gases and aerosols: methodology and application, Atmos. Chem. Phys., 10, 7017–7039, doi:10.5194/acp-10-7017-2010, 2010. 6272

Lamarque, J.-F., Shindell, D. T., Josse, B., Young, P. J., Cionni, I., Eyring, V., Bergmann, D., Cameron-Smith, P., Collins, W. J., Doherty, R., Dalsoren, S., Faluvegi, G., Folberth, G., Ghan, S. J., Horowitz, L. W., Lee, Y. H., MacKenzie, I. A., Nagashima, T., Naik, V., Plummer, D., Righi, M., Rumbold, S. T., Schulz, M., Skeie, R. B., Stevenson, D. S., Strode, S., Sudo, K., Szopa, S., Voulgarakis, A., and Zeng, G.: The Atmospheric Chemistry and Climate Model Intercomparison Project (ACCMIP): overview and description of models, simulations and climate diagnostics, Geosci. Model Dev., 6, 179–206, doi:10.5194/gmd-6-179-2013, 2013. 6266

Lee, Y. H., Lamarque, J.-F., Flanner, M. G., Jiao, C., Shindell, D. T., Berntsen, T., Bisiaux, M. M., Cao, J., Collins, W. J., Curran, M., Edwards, R., Faluvegi, G., Ghan, S., Horowitz, L. W., McConnell, J. R., Ming, J., Myhre, G., Nagashima, T., Naik, V., Rumbold, S. T., Skeie, R. B.,

GMDD
7, 6263–6325, 2014

Sudo, K., Takemura, T., Thevenon, F., Xu, B., and Yoon, J.-H.: Evaluation of preindustrial to present-day black carbon and its albedo forcing from Atmospheric Chemistry and Climate Model Intercomparison Project (ACCMIP), Atmos. Chem. Phys., 13, 2607–2634, doi:10.5194/acp-13-2607-2013, 2013. 6266

Levy, R. C., Remer, L. A., Mattoo, S., Vermote, E. F., and Kaufman, Y. J.: Second-generation operational algorithm: retrieval of aerosol properties over land from inversion of moderate resolution imaging spectroradiometer spectral reflectance, J. Geophys. Res., 112, D13211, doi:10.1029/2006JD007811, 2007. 6276

Lohmann, U. and Feichter, J.: Global indirect aerosol effects: a review, Atmos. Chem. Phys., 5, 715–737, doi:10.5194/acp-5-715-2005, 2005. 6265

Lopez, P.: Implementation and validation of a new prognostic large-scale cloud and precipitation scheme for climate and data-assimilation purposes, Q. J. Roy. Meteor. Soc., 128, 229–257, 2002. 6267

Mallet, M., Dubovik, O., Nabat, P., Dulac, F., Kahn, R., Sciare, J., Paronis, D., and Léon, J. F.: Absorption properties of Mediterranean aerosols obtained from multi-year ground-based remote sensing observations, Atmos. Chem. Phys., 13, 9195–9210, doi:10.5194/acp-13-9195-2013, 2013. 6265

Mangold, A., De Backer, H., De Paepe, B., Dewitte, S., Chiapello, I., Derimian, Y., Kacenelenbogen, M. J., Léon, F., Huneeus, N., Schulz, M., Ceburnis, D., O'Dowd, C., Flentje, H., Kinne, S., Benedetti, A., Morcrette, J.-J., and Boucher, O.: Aerosol analysis and forecast in the European Centre for Medium-Range Weather Forecasts Integrated Forecast System: 3. Evaluation by means of case studies, J. Geophys. Res., 116, D03302, doi:10.1029/2010JD014864, 2011. 6270

Marticorena, B. and Bergametti, G.: Modeling the atmospheric dust cycle: 1. Design of a soil-derived dust emission scheme, J. Geophys. Res., 100, 16415–16430, doi:10.1029/95JD00690, 1995. 6271, 6291, 6305

Masson, V., Champeaux, J., Chauvin, F., Meriguet, C., and Lacaze, R.: A global database of land surface parameters at 1-km resolution in meteorological and climate models, J. Climate, 16, 1261–1282, 2003. 6271

Masson, V., Le Moigne, P., Martin, E., Faroux, S., Alias, A., Alkama, R., Belamari, S., Barbu, A., Boone, A., Bouyssel, F., Brousseau, P., Brun, E., Calvet, J.-C., Carrer, D., Decharme, B., Delire, C., Donier, S., Essaouini, K., Gibelin, A.-L., Giordani, H., Habets, F., Jidane, M., Kerdraon, G., Kourzeneva, E., Lafaysse, M., Lafont, S., Lebeaupin Brossier, C., Lemonsu, A.,

GMDD
7, 6263–6325, 2014

Mahfouf, J.-F., Marguinaud, P., Mokhtari, M., Morin, S., Pigeon, G., Salgado, R., Seity, Y., Taillefer, F., Tanguy, G., Tulet, P., Vincendon, B., Vionnet, V., and Voldoire, A.: The SURFEXv7.2 land and ocean surface platform for coupled or offline simulation of earth surface variables and fluxes, Geosci. Model Dev., 6, 929–960, doi:10.5194/gmd-6-929-2013, 2013. 6267

Melas, D., Katragkou, E., Schulz, M., Lefever, K., Huijnen, V., and Eskes, H.: Validation report of the MACC reanalysis of global atmospheric composition Period 2003–2012, MACC-II Deliverable D_83.5, 2013. 6276, 6282, 6283

Morcrette, J.-J., Beljaars, A., Benedetti, A., Jones, L., and Boucher, O.: Sea-salt and dust aerosols in the ECMWF IFS model, Geophys. Res. Lett., 35, L24813, doi:10.1029/2008GL036041, 2008. 6270

Morcrette, J.-J., Boucher, O., Jones, L., Salmond, D., Bechtold, P., Beljaars, A., Benedetti, A., Bonet, A., Kaiser, J. W., Razinger, M., Schulz, M., Serrar, S., Simmons, A. J., Sofiev, M., Suttie, M., Tompkins, A. M., and Untch, A.: Aerosol analysis and forecast in the European Centre for Medium-Range Weather Forecasts Integrated Forecast System: forward modeling, J. Geophys. Res., 114, D06206, doi:10.1029/2008JD011235, 2009. 6268, 6269, 6270, 6273, 6276, 6290

Morcrette, J.-J., Benedetti, A., Jones, L., Kaiser, J. W., Razinger, M., and Suttie, M.: Prognostic aerosols in the ECMWF IFS: MACC vs. GEMS aerosols, ECMWF Tech. Mem. 659, ECMWF, December 2011, 2011a. 6270

Morcrette, J.-J., Benedetti, A., Ghelli, A., Kaiser, J. W., and Tompkins, A. M.: Aerosol-Cloud-Radiation Interactions and their Impact on ECMWF/MACC Forecasts, ECMWF Tech. Mem. 660, ECMWF, December 2011, 2011b. 6270

Nabat, P., Solmon, F., Mallet, M., Kok, J. F., and Somot, S.: Dust emission size distribution impact on aerosol budget and radiative forcing over the Mediterranean region: a regional climate model approach, Atmos. Chem. Phys., 12, 10545–10567, doi:10.5194/acp-12-10545-2012, 2012. 6271

Nabat, P., Somot, S., Mallet, M., Chiapello, I., Morcrette, J. J., Solmon, F., Szopa, S., Dulac, F., Collins, W., Ghan, S., Horowitz, L. W., Lamarque, J. F., Lee, Y. H., Naik, V., Nagashima, T., Shindell, D., and Skeie, R.: A 4-D climatology (1979–2009) of the monthly tropospheric aerosol optical depth distribution over the Mediterranean region from a comparative evaluation and blending of remote sensing and model products, Atmos. Meas. Tech., 6, 1287–1314, doi:10.5194/amt-6-1287-2013, 2013. 6276, 6288

GMDD
7, 6263–6325, 2014

Nabat, P., Somot, S., Mallet, M., Sevault, F., Chiacchio, M., and Wild, M.: Direct and semi-direct aerosol radiative effect on the Mediterranean climate variability using a coupled Regional Climate System Model, Clim. Dynam., doi:10.1007/s00382-014-2205-6, in press, 2014. 6288

Nabat, P., Somot, S., Mallet, M., Sanchez-Lorenzo, A., and Wild, M.: Contribution of anthropogenic sulfate aerosols to the changing Euro-Mediterranean climate since 1980, Geophys. Res. Lett., 41, 5605–5611, doi:10.1002/2014GL060798, 2014. 6288

Nabat, P., Somot, S., Mallet, M., Michou, M., Sevault, F., Driouech, F., Meloni, D., Di Sarra, A., Di Biagio, C., Formenti, P., Sicard, M., J.-Léon, F., and Bouin, M.-N., Dust aerosol radiative effects during summer 2012 simulated with a coupled regional aerosol-atmosphere-ocean model over the Mediterranean, Atmos. Chem. Phys. Discuss., submitted, 2014. 6271, 6288

Pan, X., Chin, M., Gautam, R., Bian, H., Kim, D., Colarco, P. R., Diehl, T. L., Takemura, T., Pozzoli, L., Tsigaridis, K., Bauer, S., and Bellouin, N.: A multi-model evaluation of aerosols over South Asia: Common problems and possible causes, Atmos. Chem. Phys. Discuss., 14, 19095–19147, doi:10.5194/acpd-14-19095-2014, 2014. 6272

Piriou, J.-M., Redelsperger, J.-L., Geleyn, J.-F., Lafore, J.-P., and Guichard, F.: An approach for convective parameterization with memory, in separating microphysics and transport in grid-scale equations, J. Atmos. Sci., 64, 4127–4139, 2007. 6267

Reddy, M. S., Boucher, O., Bellouin, N., Schulz, M., Balkanski, Y., Dufresne, J.-L., and Pham, M.: Estimates of global multicomponent aerosol optical depth and direct radiative perturbation in the Laboratoire de Météorologie Dynamique general circulation model, J. Geophys. Res., 110, D10S16, doi:10.1029/2004JD004757, 2005. 6271

Riahi, K., Rao, S., Krey, V., Cho, C., Chirkov, V., Fischer, G., Kindermann, G., Nakicenovic, N., and Rafaj, P.: RCP 8.5 a scenario of comparatively high greenhouse gas emissions, Climatic Change, 109, 33–57, doi:10.1007/s10584-011-0149-y, 2011. 6272

Shindell, D. T., Lamarque, J.-F., Schulz, M., Flanner, M., Jiao, C., Chin, M., Young, P. J., Lee, Y. H., Rotstayn, L., Mahowald, N., Milly, G., Faluvegi, G., Balkanski, Y., Collins, W. J., Conley, A. J., Dalsoren, S., Easter, R., Ghan, S., Horowitz, L., Liu, X., Myhre, G., Nagashima, T., Naik, V., Rumbold, S. T., Skeie, R., Sudo, K., Szopa, S., Takemura, T., Voulgarakis, A., Yoon, J.-H., and Lo, F.: Radiative forcing in the ACCMIP historical and future climate simulations, Atmos. Chem. Phys., 13, 2939–2974, doi:10.5194/acp-13-2939-2013, 2013. 6266

Szopa, S., Balkanski, Y., Schulz, M., Bekki, S., Cugnet, D., Fortems-Cheiney, A., Turquety, S., Cozic, A., Déandreis, C., Hauglustaine, D., Idelkadi, A., Lathière, J., Lefevre, F.,

GMDD
7, 6263–6325, 2014

Marchand, M., Vuolo, R., Yan, N., and Dufresne, J.-L.: Aerosol and ozone changes as forcing for climate evolution between 1850 and 2100, Clim. Dynam., 40, 2223–2250, doi:10.1007/s00382-012-1408-y, 2012. 6274

Tanré, D., Geleyn, J. F., and Slingo, J.: First results of the introduction of an advanced aerosol-radiation interaction in the ECMWF low resolution global model, in: Aerosols and Their Climatic Effects: Proceedings of the Meetings of Experts, Williamsburg, Virginia, 28–30 March 1983, edited by: Gerber, H. E. and Deepak, A., 133–177, Deepak, A., Hampton, Va., 1984. 6266

Tanré, D., Kaufman, Y. J., Herman, M., and Mattoo, S.: Remote sensing of aerosol properties over oceans using the MODIS/EOS spectral radiances, J. Geophys. Res., 102, 16971–16988, 1997. 6276

Taylor, K. E.: Summarizing multiple aspects of model performance in a single diagram, J. Geophys. Res., 106, 7183–7192, 2001. 6287, 6321

Taylor, K. E., Stouffer, R. J., and Meehl, G: A summary of the CMIP5 experiment design, available at: http://cmip-pcmdi.llnl.gov/cmip5/docs/Taylor_CMIP5_design.pdf (last access: January 2011), 2009. 6265

Textor, C., Schulz, M., Guibert, S., Kinne, S., Balkanski, Y., Bauer, S., Berntsen, T., Berglen, T., Boucher, O., Chin, M., Dentener, F., Diehl, T., Easter, R., Feichter, H., Fillmore, D., Ghan, S., Ginoux, P., Gong, S., Grini, A., Hendricks, J., Horowitz, L., Huang, P., Isaksen, I., Iversen, I., Kloster, S., Koch, D., Kirkevåg, A., Kristjansson, J. E., Krol, M., Lauer, A., Lamarque, J. F., Liu, X., Montanaro, V., Myhre, G., Penner, J., Pitari, G., Reddy, S., Seland, Ø, Stier, P., Takemura, T., and Tie, X.: Analysis and quantification of the diversities of aerosol life cycles within AeroCom, Atmos. Chem. Phys., 6, 1777–1813, doi:10.5194/acp-6-1777-2006, 2006. 6265, 6270, 6306

Tosca, M. G., Randerson, J. T., and Zender, C. S.: Global impact of smoke aerosols from landscape fires on climate and the Hadley circulation, Atmos. Chem. Phys., 13, 5227–5241, doi:10.5194/acp-13-5227-2013, 2013. 6273

Tsigaridis, K., Daskalakis, N., Kanakidou, M., Adams, P. J., Artaxo, P., Bahadur, R., Balkanski, Y., Bauer, S. E., Bellouin, N., Benedetti, A., Bergman, T., Berntsen, T. K., Beukes, J. P., Bian, H., Carslaw, K. S., Chin, M., Curci, G., Diehl, T., Easter, R. C., Ghan, S. J., Gong, S. L., Hodzic, A., Hoyle, C. R., Iversen, T., Jathar, S., Jimenez, J. L., Kaiser, J. W., Kirkevåg, A., Koch, D., Kokkola, H., Lee, Y. H., Lin, G., Liu, X., Luo, G., Ma, X., Mann, G. W., Mihalopoulos, N., Morcrette, J.-J., Müller, J.-F., Myhre, G., Myriokefalitakis, S., Ng, S., O'Donnell, D.,

GMDD
7, 6263–6325, 2014

Penner, J. E., Pozzoli, L., Pringle, K. J., Russell, L. M., Schulz, M., Sciare, J., Seland, Ø, Shindell, D. T., Sillman, S., Skeie, R. B., Spracklen, D., Stavrakou, T., Steenrod, S. D., Takemura, T., Tiitta, P., Tilmes, S., Tost, H., van Noije, T., van Zyl, P. G., von Salzen, K., Yu, F., Wang, Z., Wang, Z., Zaveri, R. A., Zhang, H., Zhang, K., Zhang, Q., and Zhang, X.: The AeroCom evaluation and intercomparison of organic aerosol in global models, Atmos. Chem. Phys. Discuss., 14, 6027–6161, doi:10.5194/acpd-14-6027-2014, 2014. 6273, 6291, 6306

Voldoire, A., Sanchez-Gomez, E., Salas y Mélia, D., Decharme, B., Cassou, C., Sénési, S., Valcke, S., Beau, I., Alias, A., Chevallier, M., Déqué, M., Deshayes, J., Douville, H., Fernandez, E., Madec, G., Maisonnave, E., Moine, M.-P., Planton, S., Saint-Martin, D., Szopa, S., Tytéca, S., Alkama, R., Bélamari, S., Braun, A., Coquart, L., and Chauvin, F.: The CNRM-CM5.1 global climate model: description and basic evaluation, Clim. Dynam., 40, 2091–2121, doi:10.1007/s00382-011-1259-y, 2012. 6267, 6268, 6274, 6290

van Vuuren, D. P., Edmonds, J., Kainuma, M., Riahi, K., Thomson, A., Hibbard, K., Hurtt, G. C., Kram, T., Krey, V., Lamarque, J. F., Masui, T., Meinshausen, M., Nakicenovic, N., Smith, S. J., and Rose, S. K.: The representative concentration pathways: an overview, Climatic Change, 109, 5–31, doi:10.1007/s10584-011-0148-z.

Zhang, K., Wan, H., Liu, X., Ghan, S. J., Kooperman, G. J., Ma, P.-L., Rasch, P. J., Neubauer, D., and Lohmann, U.: Technical Note: On the use of nudging for aerosol–climate model intercomparison studies, Atmos. Chem. Phys., 14, 8631–8645, doi:10.5194/acp-14-8631-2014, 2014. 6274

GMDD
7, 6263–6325, 2014

Table 1. Summary of ARPEGE-Climat simulations performed.

Name	Forcing	Duration (years)	Dust scheme
FreSim	2004	10	Ginoux et al. (2001)
NudSim	2004	1	Ginoux et al. (2001)
FreSimd2	2004	10	Marticorena and Bergametti (1995) Kok (2011)
NudSimd2	2004	1	Marticorena and Bergametti (1995) Kok (2011)
FreSimd2_Trans	1993–2012	20	Marticorena and Bergametti (1995) Kok (2011)
NudSimd2_Trans	1993–2012	20	Marticorena and Bergametti (1995) Kok (2011)

GMDD
7, 6263–6325, 2014

Table 2. Totals emitted for static emissions, including those used for the 2004 simulations, the 2003–2012 transient simulations, the MACC Reanalysis, and totals reported in the literature. BC, OM and SOA in Tg yr^{-1}, all sulfur species in Tg(SO_2) yr^{-1}.

Sim./Litt.		Sim. 2004	Sim. 1993–2012 Range	MACC Rean. 2004	Litterature
Species	Source				
BC	Tot. Sour.	10.3	9.1–11.8	6.2	12 ± 3[a], 15 ± 14[b]
	Bio. Burn.	5.0	4.1–6.5		
	Oth. Sour.	5.3	5.0–5.3		
OM	Tot. Sour.	117.3	105.4–139.4	48.5	97 ± 25[a], 119 ± 111[b]
	Bio. Burn.	63.2	52.4–85.2		
	SOA	34.7	34.7		19 (13–121)[c]
	Oth. Sour.	19.4	18.3–19.5		
SO_2	Tot. Sour.	90.6	82.4–96.1	101.5	
	Bio. Burn.	3.3	2.4–4.4		
	Volcan.	12.0	12.0		
	Oth. Sour.	75.6	68.0–79.7		
DMS	Oceans.	27.9	27.9	0	
H_2S	Tot. Sour.	3.8	3.4–4.0	0	
SO_4	Tot. Sour.	6.0	5.6–6.2	0	
All SO_4 prec.	Tot. Sour.	128.0	119.3–133.6	101.5	119 ± 26[a]

[a] AeroCom mean $\pm\sigma$ (intermodel), Textor et al. (2006) Table 10.
[b] Mean $\pm\sigma$ (intermodel), Huneeus et al. (2012) Table 5.
[c] Tsigaridis et al. (2014) mean and range from models.

GMDD
7, 6263–6325, 2014

Table 3. Upper part of the Table: dust emissions (Tg yr^{-1}) over regions defined in Huneeus et al. (2011), for the FreSim and FreSimd2 simulations (mean over the 10 repeated 2004 years), the NudSim and NudSimd2 simulations (year 2004), the MACC Reanalysis (2003–2012 mean), and results from 15 AEROCOM models analysed in Huneeus et al. (2011), median, min, and max values. In blue, totals lower than the AEROCOM min, in red, totals higher than the AEROCOM max. Lower part of the Table: global sea-salt emissions (Pg $year^{-1}$), with a range from Grythe et al. (2014).

Dust Tg yr^{-1} Region	FreSim/FreSimd2	NudSim/NudSimd2	MACC Rean.	AEROCOM Median (min–max)
Global	379/4236	258/3618	313	1586 (487–3943)
North Africa	112/1298	66/1039	88	792 (204–2888)
Middle East	66/659	51/579	37	128 (26–531)
Asia	76/468	62/407	75	137 (27–873)
South America	0/48	0/46	2	10 (0–186)
South Africa	5/77	3/51	12	12 (3–57)
Australia	37/290	20/175	47	31 (9–90)
North America	1/11	1/13	16	2 (2–286)
Sea-Salt				
Pg $year^{-1}$	FreSim	NudSim	MACC Rean.	Range Grythe et al. (2014)
Global	59.9	51.6	64.2	1.8 to 605.0

GMDD
7, 6263–6325, 2014

Table 4. Constants used in the aerosol scheme, in black values of the MACC reanalysis, in red values changed in our simulations: Eff. for scav.: efficiency for scavenging – Eff. bc. r.: Efficiency for below-cloud scavenging rain – Eff. bc. s.: Efficiency for below-cloud scavenging snow – Reev. const.: reevaporation constant – Dry dep. vel.: dry deposition velocity ($m\,s^{-1}$), ocean, land, ice – Eff. for sedim.: efficiency for sedimendation ($m\,s^{-1}$) – Frac. phil/phob: fraction hydrophilic/hydrophopic – Rate phob/phil: transformation rate from hydrophopic to hydrophilic – DD emis pot.: dust emission potential ($kg\,s^2\,m^{-5}$), bin radius (µm).

Constant	BCphil	BCphob	OMphil	OMphob	DDbin01	DDbin02	DDbin03	SSbin01	SSbin02	SSbin03	SO_4	SO_2
Eff. for scav. *D*	0.8/0.1	0.5/0	0.8/0.1	0.5/0		0.5			0.5/0.2		0.5/0.2	0
Eff. bc. r. αr			0.001			0.001			0.001		0	
Eff. bc. r. αs			0.01			0.01			0.01		0	
Reev. const. RFRAER			0.5			0.5			0.5		0.5	–
Rain radius (m) R_R			0.001			0.001			0.001		0.001	–
Snow radius (m) R_S			0.001			0.001			0.001		0.001	–
Dry dep. vel. V_{docean}			0.28E-02/0.1E-02		0.1E-02/ 0.15E-02	0.11E-01/ 0.07E-01	0.145E-01	0.1E-02/ 0.15E-02	0.11E-01/ 0.07E-01	0.145E-01	0.05E-02	0.70E-02/ 0.15E-01
V_{dland}			0.14E-02/0.1E-02		0.1E-02/ 0.15E-02	0.11E-01/ 0.07E-01	0.145E-01	0.1E-02/ 0.15E-02	0.11E-01/ 0.07E-01	0.145E-01	0.25E-02	0.30E-02/ 0.50E-02
V_{dice}			0.17E-02/0.1E-02		0.1E-02/ 0.15E-02	0.11E-01/ 0.07E-01	0.145E-01	0.1E-02/ 0.15E-02	0.11E-01/ 0.07E-01	0.145E-01	0.25E-02	0.20E-02/ 0.30E-02
Eff. for sedim. v_s			0.10E-02/0		0.6904E-04/0	0.1982E-03/0	0.1962E-02	0.24E-04/0	0.195E-02/0	0.180E-01	0.05E-02/0	0
Frac. phil/phob Rxxpppp	0.2/0.8	0.8/0.2	0.5	0.5	–	–	–	–	–	–	–	–
Rate phob/phil RGRATE			7.1E-06		–	–	–	–	–	–	–	–
DD emis pot. S	–	–	–	–		2.0E-11/1.0E-11		–	–	–	–	–
Bin radius ZMMD	–	–	–	–	0.32/0.2	0.75/1.67	9.0/11.6	0.30	3.00	10.00	–	–

GMDD
7, 6263–6325, 2014

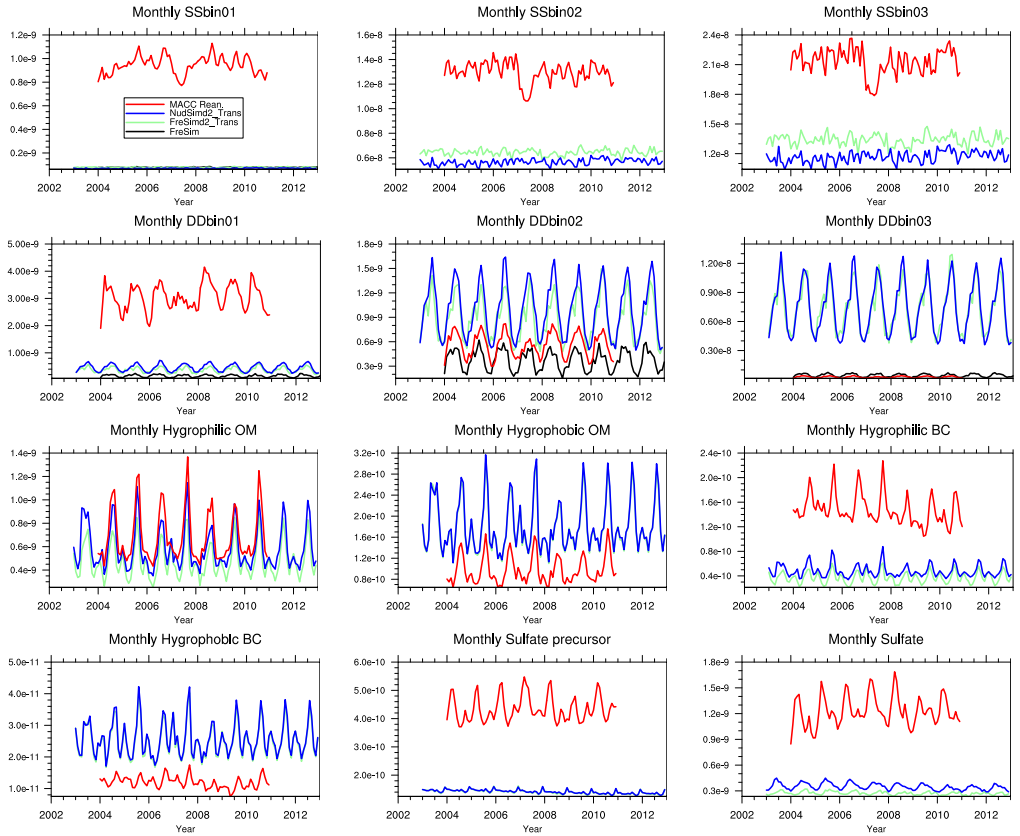

Figure 1. Time series of monthly mean global bin concentrations ($kg\,kg^{-1}$) in the lower troposphere (1000 to 500 hPa layer) for the FreSimd2_Trans (green line), NudSimd2_Trans (blue line), and MACC Reanalysis (red line). In addition, dust bin concentrations are added for the FreSim simulation (black line, 2004 repeated 10 times). The 12 "bins" of the aerosol scheme are shown.

GMDD
7, 6263–6325, 2014




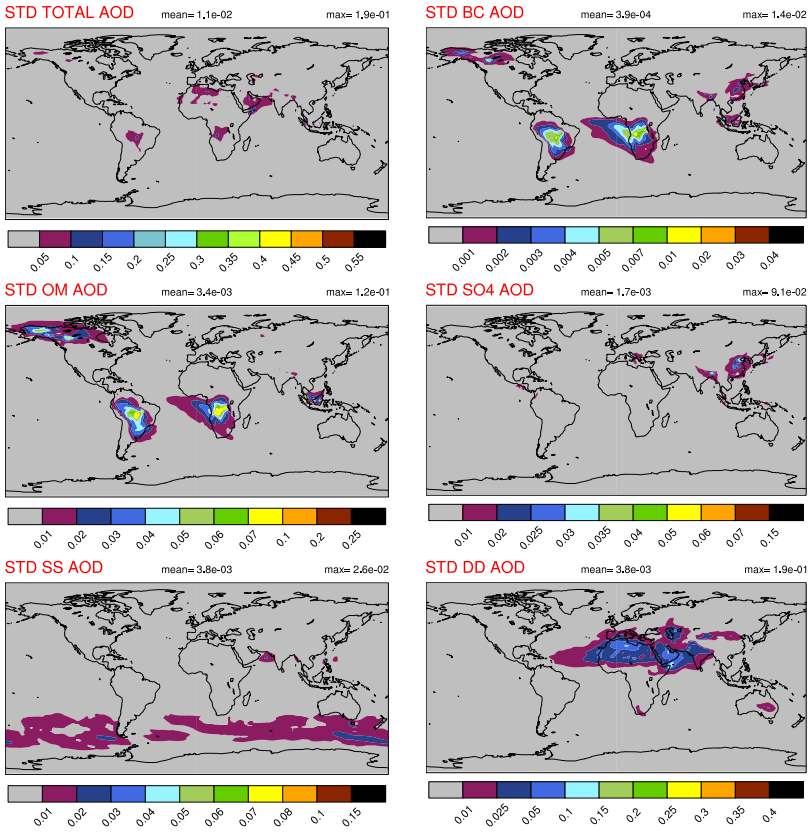

Figure 2. Mean standard deviation for JJA for the FreSimd2 simulation, as a representation of the ARPEGE-Climat internal variability, of the total, BC, OM, sulfate, SS, and DD AODs. Color scales are the same as in Fig. 5 and 7.

GMDD
7, 6263–6325, 2014

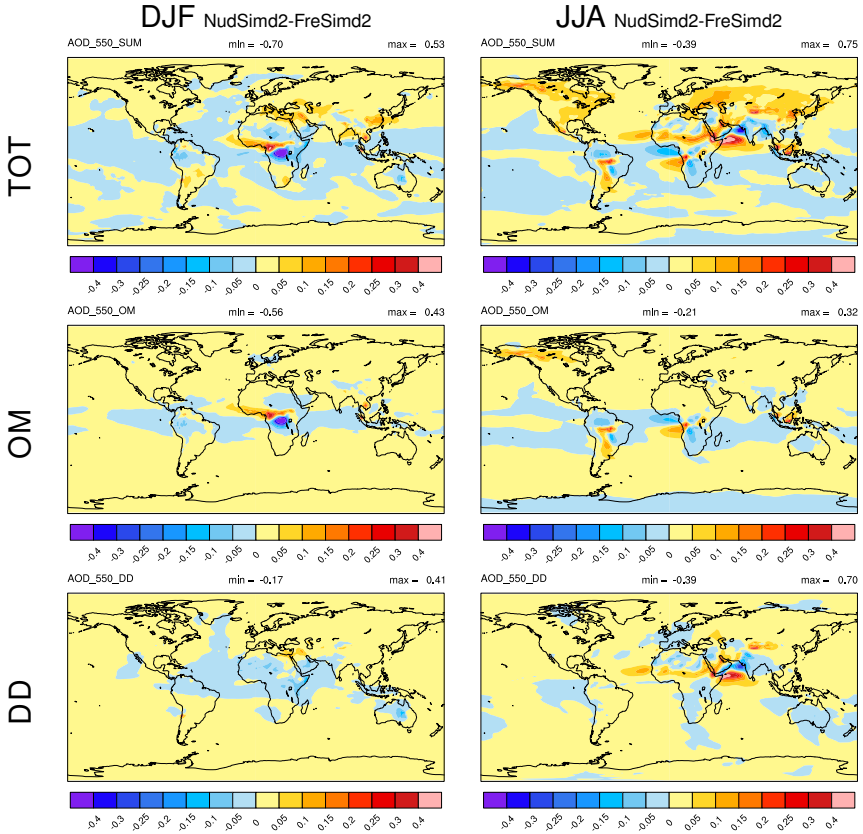

Figure 3. Differences in AOD between the NudSimd2 and the FreSimd2 simulations, for DJF (left column) and JJA (right column), and for total AOD (first row), OM AOD (second row) and DD AOD (last row).

GMDD
7, 6263–6325, 2014

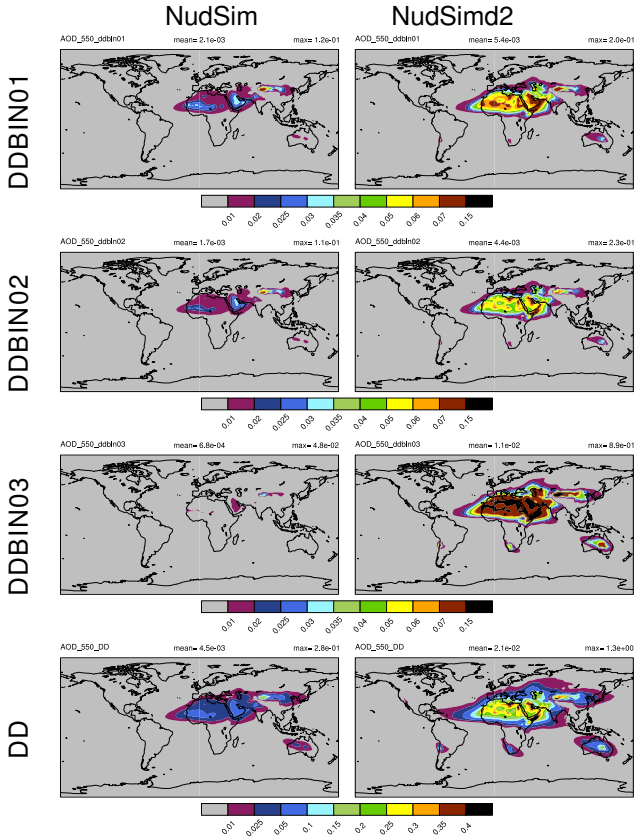

Figure 4. Mean 2004 dust AOD for the NudSim (first column), and the NudSimd2 (second column) simulations, for the three dust bins, from the smallest (first row) to the largest (third row), and total DD AOD in fourth row.

GMDD
7, 6263–6325, 2014

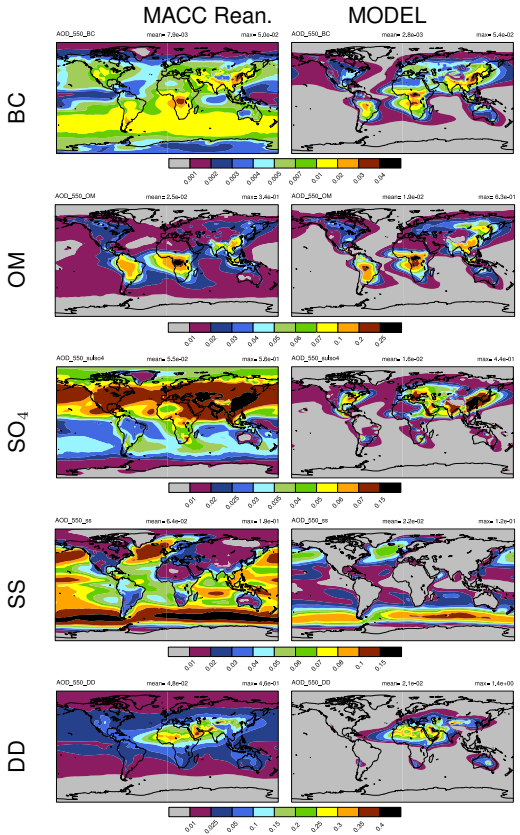

Figure 5. Mean AOD (2003–2012) for the MACC Reanalysis (first column), and the NudSimd2_Trans simulation (second column), for BC, OM, sulfate, SS and DD.

GMDD
7, 6263–6325, 2014

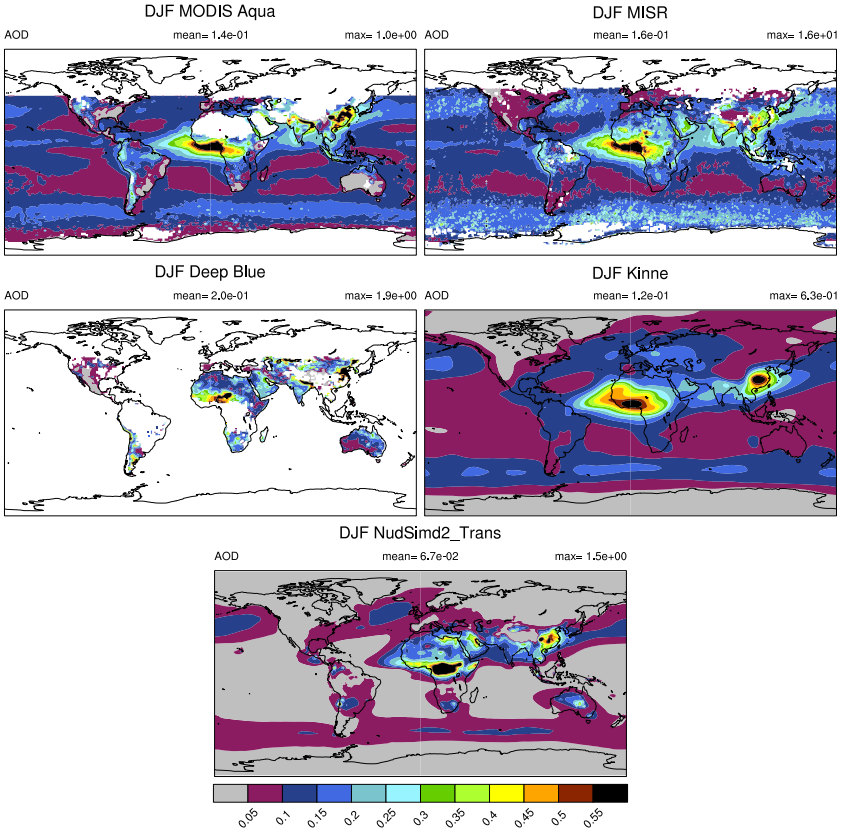

Figure 6. Mean DJF 2003–2012 total AOD for the MODIS Aqua, MISR, MODIS Deep-Blue and Kinne et al. (2013) data sets (from the top in the direction of reading), and from the NudSimd2_Trans simulation (third row).

GMDD
7, 6263–6325, 2014

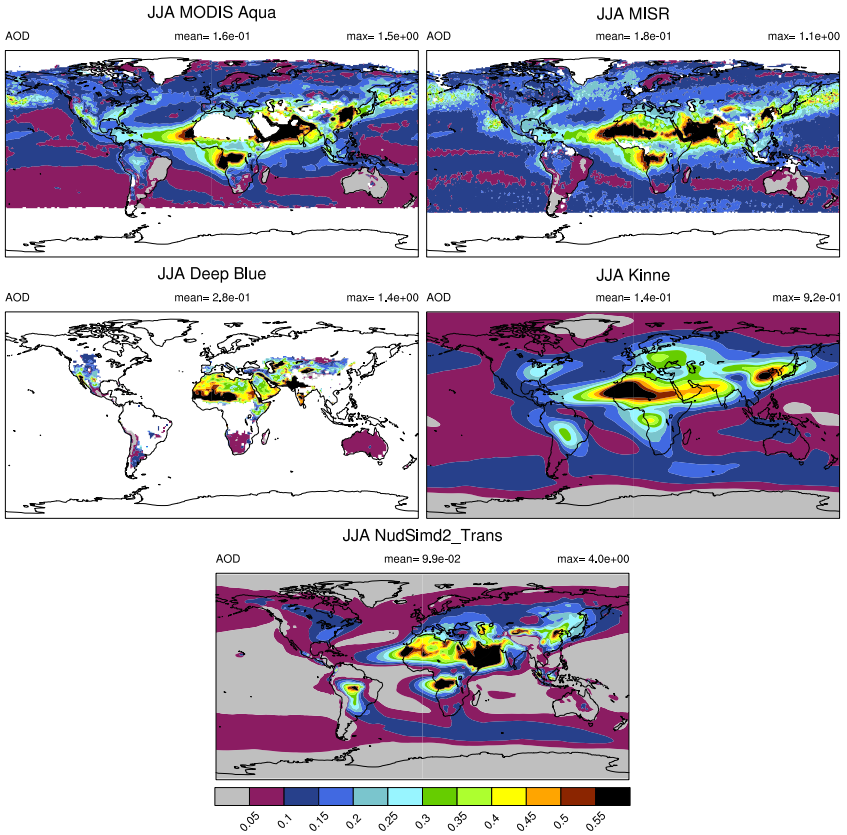

Figure 7. Same as Fig. 6, for JJA.

GMDD
7, 6263–6325, 2014

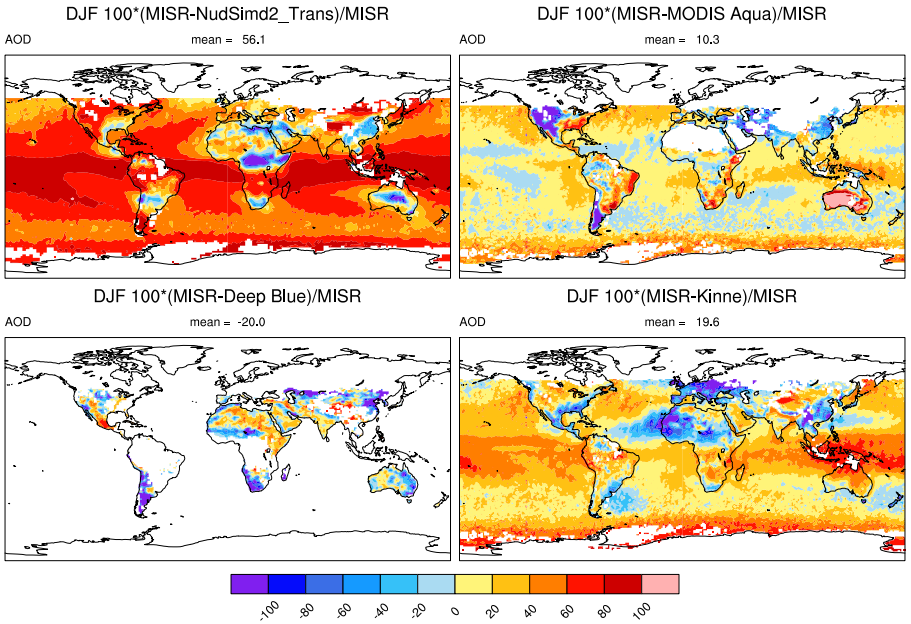

Figure 8. DJF total AOD mean relative differences (2003–2012): 100(MISR – x)/MISR, with x = NudSimd2_Trans first row/column, and x = Modis Aqua or x = MODIS Deep Blue or x = Kinne et al. (2013) in the direction of reading.

GMDD
7, 6263–6325, 2014

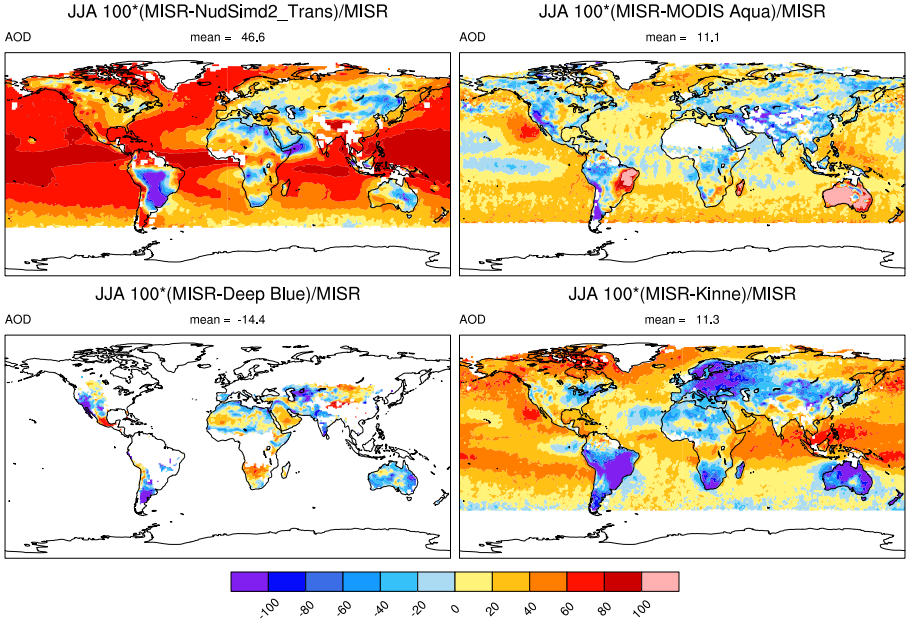

Figure 9. Same as Fig. 8, for JJA.

GMDD
7, 6263–6325, 2014

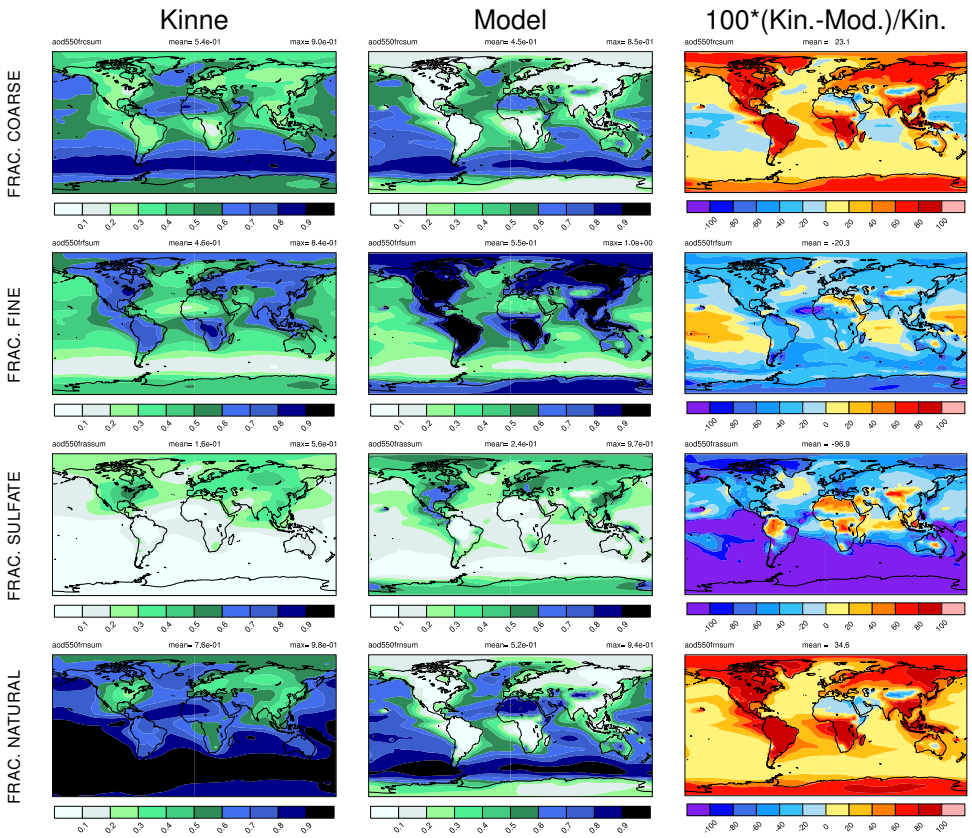

Figure 10. Mean annual fractional AOD from the Kinne et al. (2013) climatology (first colunm), NudSimd2_Trans simulation (1996–2005) (second column) and relative difference between the two data sets: fraction of coarse mode (first row), of fine mode (second row), of sulfate (third row), and of natural aerosols (fourth row).

GMDD
7, 6263–6325, 2014

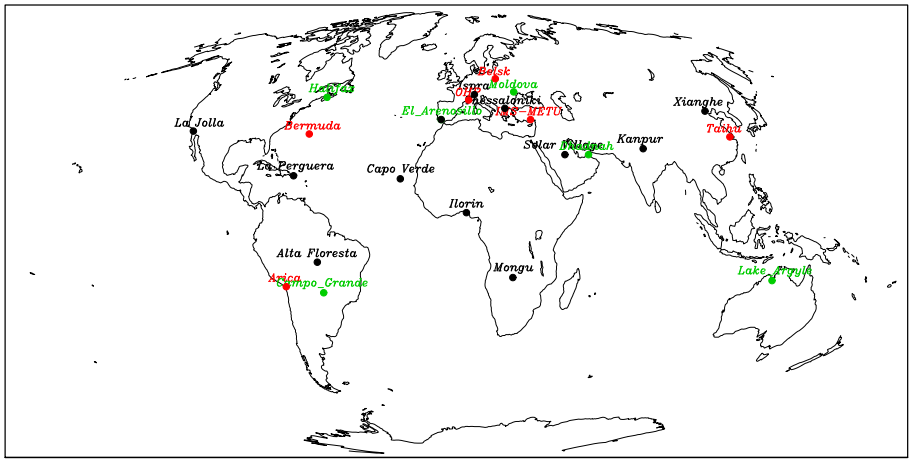

Figure 11. Location of the AERONET stations presented in Fig. 12, names in black, and in Fig. 14, names in red for poor performance, in green for good performance.

GMDD
7, 6263–6325, 2014

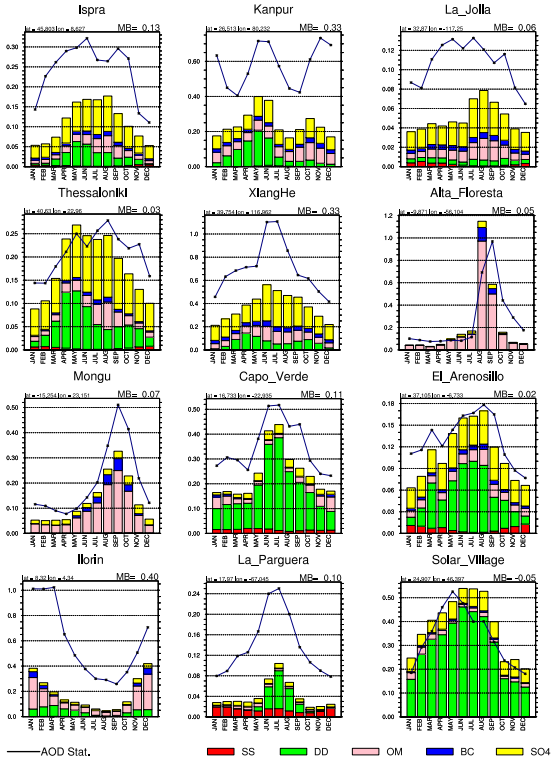

Figure 12. Monthly climatology of AOD, computed from all years of available data, for the AERONET stations of Cesnulyte et al. (2014). Total observed AOD, and SO_4, BC, OM, DD and SS AODs from the NudSimd2_Trans simulation are displayed.

GMDD
7, 6263–6325, 2014

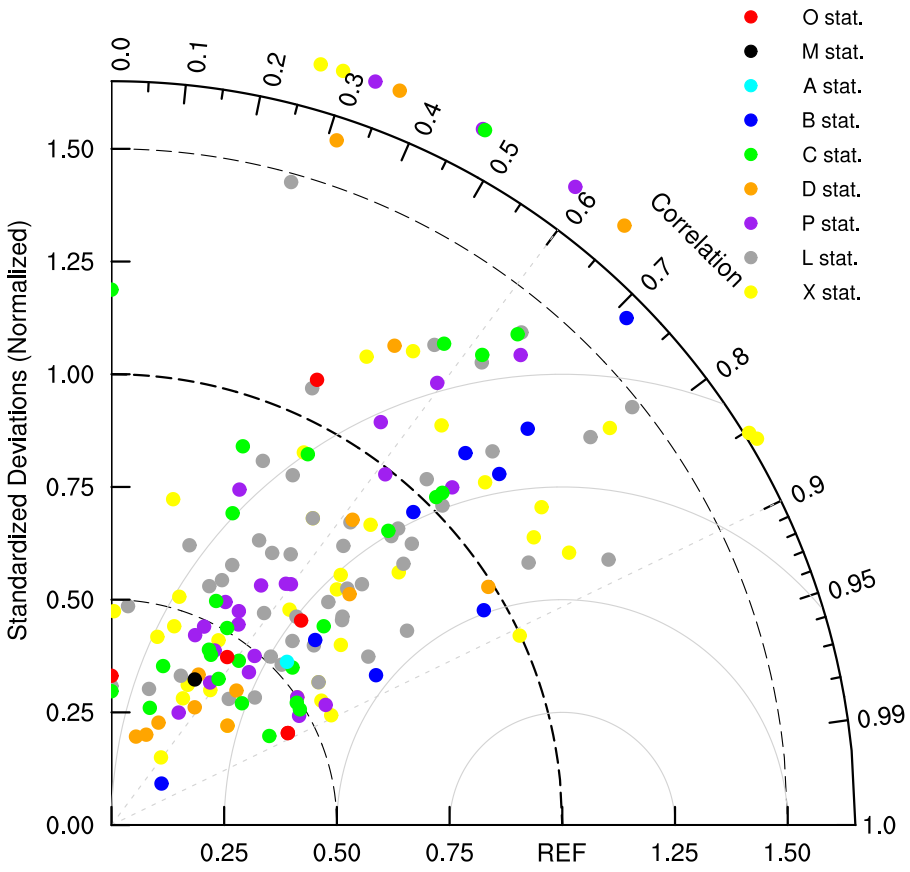

Figure 13. Taylor diagram (Taylor, 2001) for the AOD monthly time series of 166 AERONET stations and ouputs from the NudSimd2_Trans simulation (see text for details). The qualification of the stations is that of Kinne et al. (2013) indicating the site dominant aerosol category (O, ocean; M, mountain; A, polar; B, biomass; C, coastal; D, dust; P, polluted, L, land), and X, no qualification.

GMDD
7, 6263–6325, 2014

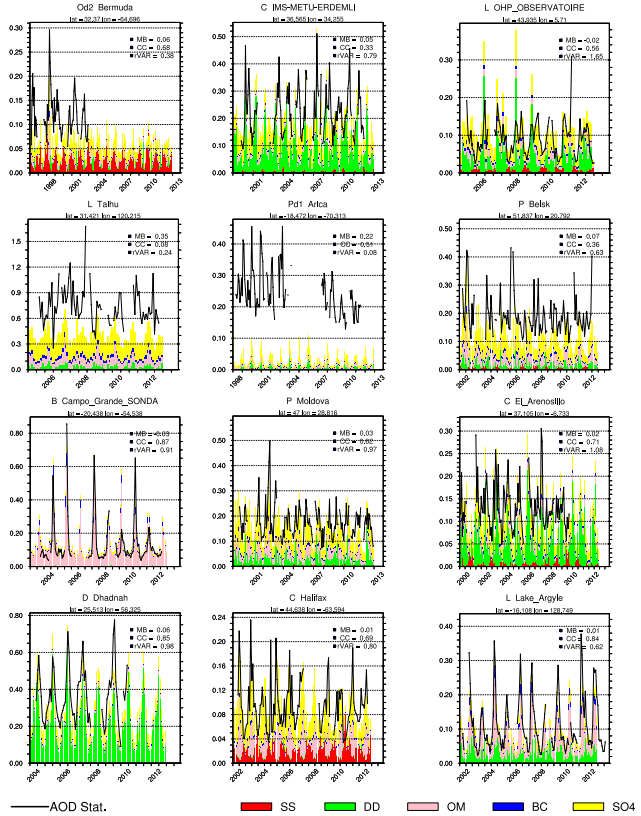

Figure 14. Times series of monthly AODs, for a selection of poorly performing AERONET stations, first six images, and of good performing AERONET stations, last six images, according to the Taylor diagram of Fig. 13. The same AODs as in Fig. 12 are shown. rVar: ratio of modelled versus observed standard deviations, CC: correlation coefficient between observed and modelled time series, and MB: mean bias.

GMDD
7, 6263–6325, 2014

A prognostic aerosol scheme in CNRM-CM

M. Michou et al.

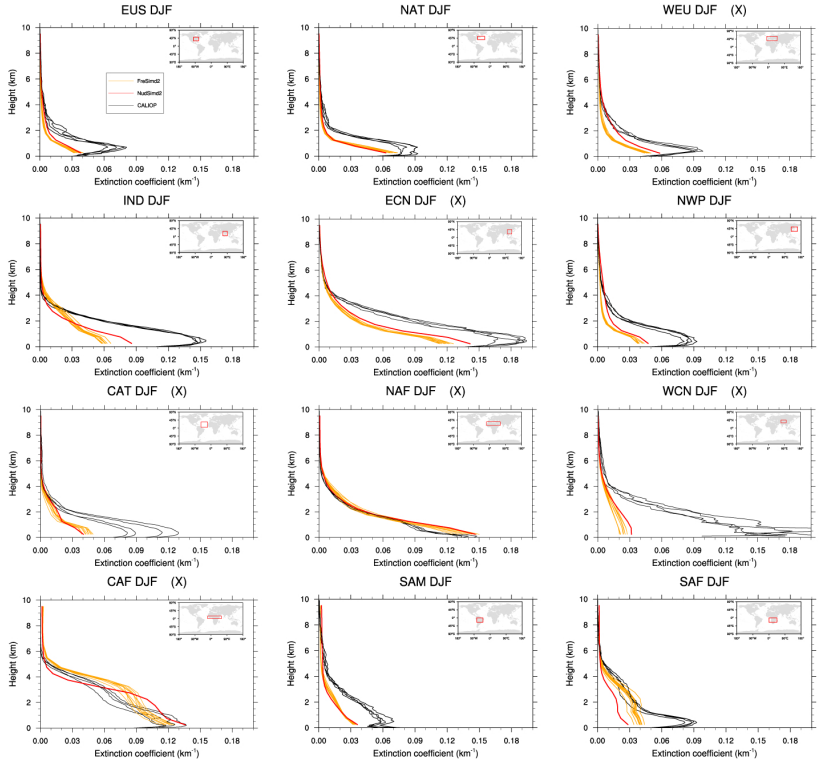

Figure 15. Mean DJF vertical profiles of extinction coefficients (km^{-1}) for total aerosols, for the FreSimd2 simulation (orange lines) for 2004, repeated 10 times, the NudSimd2 simulation (red line), and for individual years of the CALIOP 3-D product (black lines), over 12 regions of the globe, as in Koffi et al. (2012) (see in top right corners of individual figures). (X): regions also presented in Fig. 17.

GMDD
7, 6263–6325, 2014

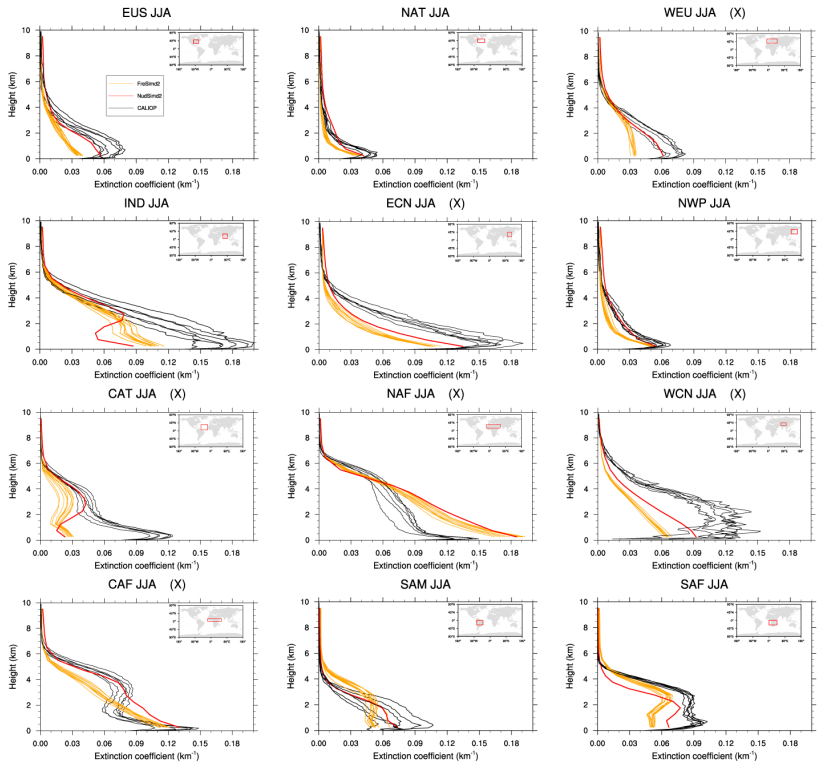

Figure 16. Same as Fig. 15, for the JJA season.

GMDD
7, 6263–6325, 2014

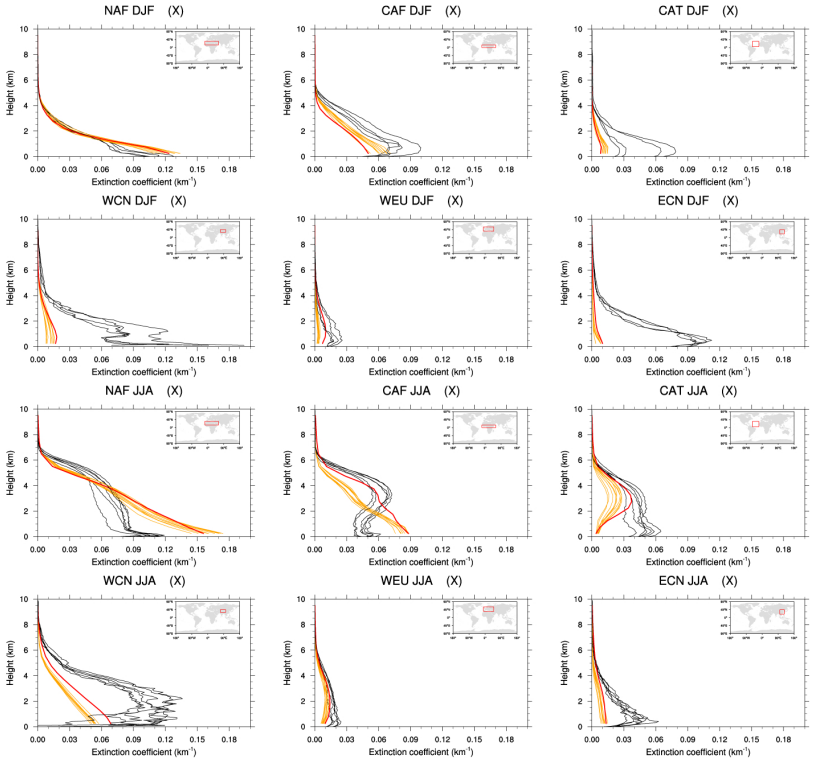

Figure 17. Mean vertical profiles of extinction coefficients (km^{-1}) for the dust aerosol, for the FreSimd2 simulation (orange lines) for 2004, repeated 10 times, the NudSimd2 simulation (red line), and for individual years of the CALIOP 3-D product (black line), over 6 regions of the globe with dust aerosols, as in Koffi et al. (2012), for DJF (rows 1 and 2) and JJA (rows 3 and 4).

GMDD
7, 6263–6325, 2014